# Understanding the long-term spectral variability of Cygnus X-1 with BATSE and ASM observations

Andrzej A. Zdziarski[1], Juri Poutanen[2,3], William S. Paciesas[4] and Linqing Wen[5]

## ABSTRACT

We present a comprehensive analysis of all observations of Cygnus X-1 by the *CGRO*/BATSE (20–300 keV) and by *RXTE*/ASM (1.5–12 keV) until 2002 June, including $\sim$ 1200 days of simultaneous data. We find a number of correlations between fluxes and hardnesses in different energy bands. In the hard (low) spectral state, there is a negative correlation between the ASM 1.5–12 keV flux and the hardness at any energy. In the soft (high) spectral state, the ASM flux is positively correlated with the ASM hardness but uncorrelated with the BATSE hardness. In both spectral states, the BATSE hardness correlates with the flux above 100 keV, while it shows no correlation with the 20–100 keV flux. At the same time, there is clear correlation between the BATSE fluxes below and above 100 keV. In the hard state, most of the variability can be explained by softening the overall spectrum with a pivot at $\sim$ 50 keV. There is also another, independent variability pattern of lower amplitude where the spectral shape does not change when the luminosity changes. In the soft state, the variability is mostly caused by a variable hard (Comptonized) spectral component of a constant shape superimposed on a constant soft blackbody component. These variability patterns are in agreement with the dependencies of the rms variability on the photon energy in the two states.

We also study in detail recent soft states from late 2000 till 2002. The last of them has lasted so far for $>$ 200 days. Their spectra are generally harder in the 1.5–5 keV band and similar or softer in the 3–12 keV band than the spectra of the 1996 soft state whereas the rms variability is stronger in all the ASM bands. On the other hand, the 1994 soft state transition observed by BATSE appears very similar to the 1996 one.

We interpret the variability patterns in terms of theoretical Comptonization models. In the hard state, the variability appears to be driven mostly by changing flux in seed photons Comptonized in a hot thermal plasma cloud with an approximately constant power supply. In the soft state, the variability is consistent with flares of hybrid, thermal/nonthermal, plasma with variable power above a stable cold disk. The spectral and timing differences between the 1996 and 2000–02 soft states are explained by a decrease of the color disk temperature. Also, based on broad-band pointed observations simultaneous with those of the ASM and BATSE, we find the intrinsic bolometric luminosity increases by a factor of $\sim$ 3–4 from the hard state to the soft one, which supports models of the state transition based on a change of the accretion rate.

*Subject headings:* binaries: general — black hole physics — stars: individual (Cygnus X-1) — X-rays: observations — X-rays: stars

[1]Centrum Astronomiczne im. M. Kopernika, Bartycka 18, 00-716 Warszawa, Poland; aaz@camk.edu.pl

[2]Astronomy Division, P.O.Box 3000, 90014 University of Oulu, Finland; juri.poutanen@oulu.fi

[3]Stockholm Observatory, 10691 Stockholm, Sweden

[4]Department of Physics, National Space Science and Technology Center, University of Alabama in Huntsville, Huntsville, AL 35899, USA; Bill.Paciesas@msfc.nasa.gov

[5]Center for Space Research, Massachusetts Institute of Technology, Cambridge, MA 02139; lwen@ligo.caltech.edu

## 1. Introduction

Cygnus X-1 is an archetypical black-hole X-ray binary discovered in 1964 (Bowyer et al. 1965). Due to its brightness and the persistency of emission, its observational and theoretical studies have been of great importance for understanding of the process of accretion onto black holes in general.

A specific important tool for testing theoretical models is the study of spectral variability. Pointed observations of Cygnus X-1 with X-ray and $\gamma$-ray telescopes have provided detailed information about its broad-band spectra (Gierliński et al. 1997, hereafter G97, Gierliński et al. 1999, hereafter G99, Di Salvo et al. 2001, hereafter D01, Frontera et al. 2001, hereafter F01, McConnell et al. 2002, hereafter M02), and its short time scale variability (e.g., Revnivtsev, Gilfanov, & Churazov 2000; Maccarone, Coppi, & Poutanen 2000). However, many black hole sources, including Cygnus X-1, also show dramatic spectral changes such as spectral transitions which occur on the time scales of weeks. Understanding the causes of these variations may require long uninterupted observations which are not available. The only observationally possible alternative is to monitor a source by all-sky monitors such as the ASM detectors aboard *RXTE* and the BATSE detectors aboard *CGRO*.

Cygnus X-1 is an excellent target for such studies. It has been monitored by the ASM since 1996, and by the BATSE from 1991 to 2000. During almost 5 years (1996–2000) the monitoring was simultaneously by both detectors. Spectral variability in the ASM data alone have been studied by Wen, Cui, & Bradt (2001), Reig, Papadakis, & Kylafis (2002) and Smith, Heindl, & Swank (2002), and some aspects of spectral variability in the BATSE data have been studied by Crary et al. (1996). Some partial analyses of joint ASM-BATSE variability have been done by Zhang et al. (1997, hereafter Z97) for the 1996 state transition, and by Brocksopp et al. (1999a). Here we present a comprehensive joint analysis of spectral variability in the full currently available ASM data and of all of the BATSE data.

## 2. Data analysis

To ensure both a sufficient overlap between the observations by ASM and by BATSE and sufficient statistics, we have chosen to use data binned on one-day timescale. The ASM data (average daily count rates and their standard errors) have been taken from the public database at xte.mit.edu/ASM_lc.html. The data analyzed here cover the time interval from 1996 January 5 to 2002 June 6 (MJD 50087–52431), yielding 2127 days with usable measurements. In order to convert counts to energy units, we have constructed our own matrix based on comparison with pointed observations taken on the days with the ASM coverage, see Appendix A. In this way, we obtain energy fluxes in the photon energy, $E$, ranges of 1.5–3 keV, 3–5 keV, and 5–12 keV.

For the BATSE data, we generally followed the standard Earth occultation analysis methodology (Harmon et al. 2002). Counting rate spectra from individual occultation steps were averaged over one-day intervals. Energy fluxes in the 20–100 keV and 100–300 keV ranges were derived for each day by fitting a power-law spectrum (with variable photon spectral index, $\Gamma$, defined by the photon flux $\propto E^{-\Gamma}$) separately to the hardware channel ranges that corresponded most closely to the chosen energy intervals. To minimize interference from Cygnus X-3, we excluded data from days on which the angle between Cygnus X-3 and the closest point on the Earth's limb at the time of Cygnus X-1 occultation was $< 2.5^\circ$. We also excluded days on which fewer than four occultation steps were measured, since these are more likely to be affected by systematic errors.

The above procedure yields 2729 days with usable data from 1991 April 25 to 2000 May 22 (MJD 48371–51686). In Appendix A, we compare the BATSE data with those from the same pointed measurements as used for the ASM, and find them to be in a good general agreement.

The data sets above include 1187 days of usable data with simultaneous ASM-BATSE coverage. Using these data, we study here correlations between the ASM and BATSE fluxes and spectral slopes.

Often, hardness of spectra is described by the ratio of count rates or fluxes, $R$, in two adjacent channels. However, even if energy fluxes are used, this value depends on the width of the channels. To describe the hardness in a more objective way, we define here the effective photon power-law spectral index, $\Gamma$, by the condition of the ratio of the

energy fluxes in the power law spectrum, $R$, being equal to that in the observed spectrum. This index is analogous to colors used in stellar astrophysics. When two adjacent channels have boundary energies of $E_1 < E_2 < E_3$, the relationship between $\Gamma$ and $R$ is given by,

$$R = \begin{cases} \frac{E_3^{2-\Gamma} - E_2^{2-\Gamma}}{E_2^{2-\Gamma} - E_1^{2-\Gamma}}, & \Gamma \neq 2; \\ \frac{\ln E_3/E_2}{\ln E_2/E_1}, & \Gamma = 2. \end{cases} \quad (1)$$

The uncertainty of $\Gamma$ is given by the propagation of errors, $\Delta\Gamma = \Delta R/|\mathrm{d}R/\mathrm{d}\Gamma|$ where $\Delta R$ is the uncertainty of $R$. This allows us to obtain two effective indices for the ASM data, and one for BATSE. The BATSE effective index has a substantially better accuracy than either of the fitted BATSE indices.

## 3. Lightcurves

Figure 1a presents the 1.5–12 keV ASM and 20–300 keV BATSE energy flux light curves. We have rebinned the original ASM and BATSE one-day average data to assure that the error on each flux point is $< 10\%$ and $< 20\%$, respectively. This reduces the number of data points by only 5 and 7, respectively, and the relative accuracy of most of the values in Figure 1a is much better than the above ones. Figure 1b shows the corresponding hardness in the 3–12 keV and 20–300 keV bands, as given by the effective index of equation (1). We have chosen here the 3–12 keV index in order to avoid the effect of variable absorption by the line-of-sight matter, which affects mostly the spectrum below 3 keV.

In Figure 1, we see a soft-state transition in 1994, observed by both BATSE and OSSE (e.g., G99), very similar in form to the famous state transition of the year 1996 (Z97), as illustrated in more detail in Figure 2. Unfortunately, Cygnus X-1 was not observed at lower energies during this transition.

During the simultaneous operation of ASM and BATSE, we see the well-known overall anticorrelation of the fluxes from the two instruments. Interestingly, the 3–12 keV ASM index was rather similar to the BATSE one during the 1996 soft state. We also in Figure 1a a number of flares in the ASM flux which were *not* accompanied by any significant drops in the BATSE flux.

In addition to the 1996 soft state, we also see three shorter episodes when the ASM flux became high and its spectrum very soft, with $\Gamma(3\text{–}12\,\mathrm{keV}) > 2.4$, around MJD 51850, 51900, and 51940, reported by Cui, Feng, & Ertmer (2002). More recently, another soft state lasting for about two months occured around MJD $\sim$ 52150–52210. After this, Cygnus X-1 went to an intermediate [i.e., still soft, with $\Gamma(3-12\,\mathrm{keV}) \gtrsim 2$] state for about a month. This was followed by yet another occurence of the soft state, which started around MJD 52230 and has lasted almost continuously (with some short intervals of an intermediate state around MJD 52350) for $\sim$ 200 days so far, i.e., much longer than other state transitions of Cygnus X-1 observed so far. These recent state transitions are shown in detail in Figure 3. It is worth noticing that the spectrum during the last soft state was substantially softer than during the 1996 soft state, in the range of $\Gamma(3-12\,\mathrm{keV}) \sim 3$–3.5. Very interestingly, the spectrum since MJD 52160 until now (MJD 52431), i.e., for $> 270$ days, has shown $\Gamma(3-12\,\mathrm{keV}) \gtrsim 2$, i.e., much softer than the usual $\Gamma(3\text{–}12\,\mathrm{keV}) \sim 1.7$. Unfortunately, no monitoring at higher energies was available after MJD 51686, including those highly interesting state transitions.

We note that there have been recent reports of short (with duration $\ll 1$ day), very strong, flares from the direction of Cygnus X-1 measured at photon energies $\gtrsim 20$ keV, at which range the flux exceeded the typical, hard-state, flux by a factor of $\sim 10$ (Stern, Beloborodov, & Poutanen 2001; Golenetskii et al. 2002). These flares occured on MJD 49727, 49801, 51289 and 52329. We have looked into characteristics of the lightcurves around those days, and have found, unfortunately, no common characteristic that would allow some insight into the nature of the flares. For example, the last event occured in a soft state whereas the three previous ones, in hard states.

## 4. Spectral Correlations

### 4.1. The ASM data

Based on the variability from the ASM, we distinguish here three main spectral states. We define the soft and hard states by the conditions (see Fig. 1) of $\Gamma(3-12\,\mathrm{keV}) > 2.4$, $< 2.1$, respectively, and an intermediate state by $\Gamma(3-12\,\mathrm{keV}) = 2.1$–2.4. Our definition of the soft state corresponds, e.g.,

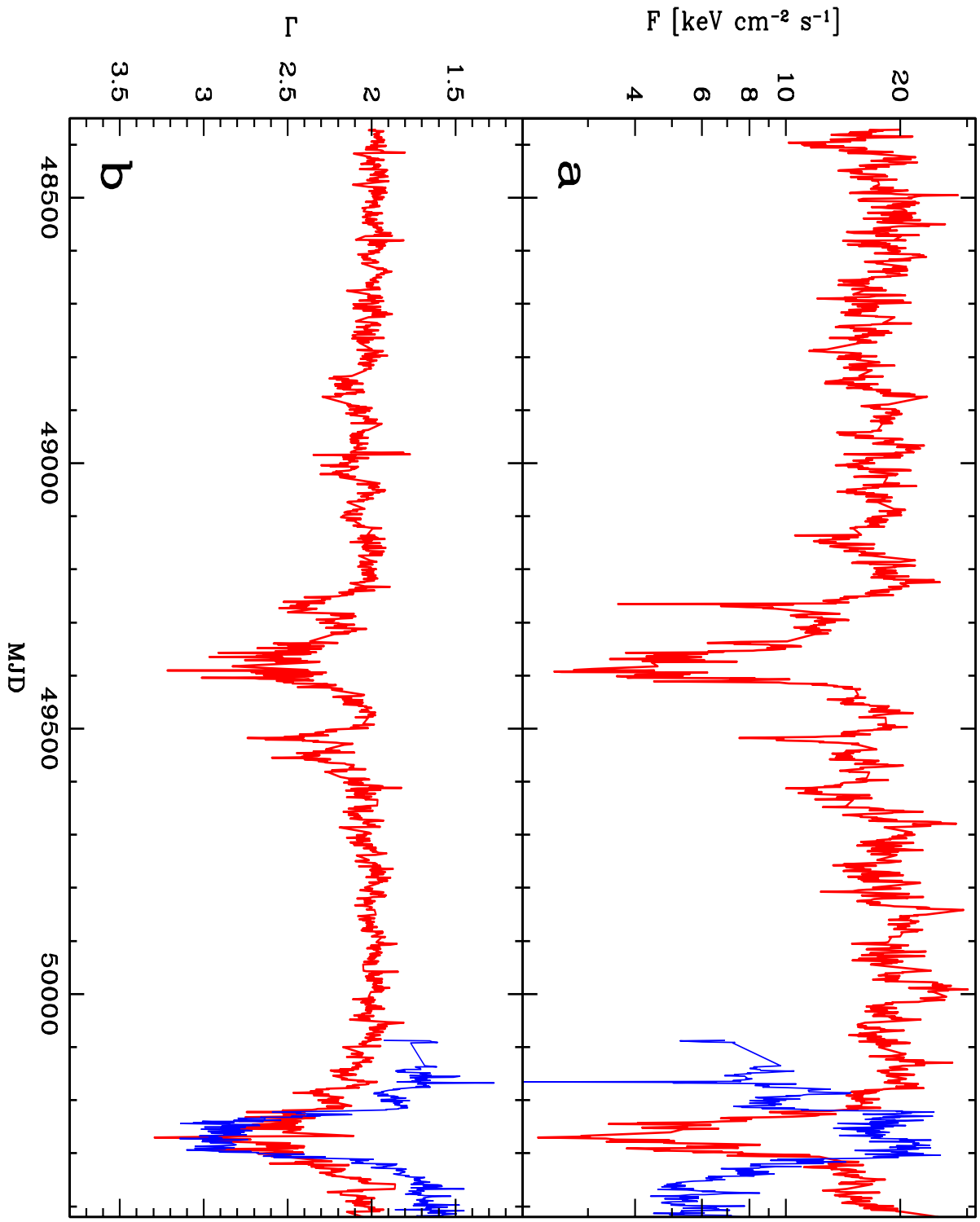


Fig. 1.— (a) Light curves of Cygnus X-1 as observed by the *RXTE*/ASM and *CGRO*/BATSE. Thin blue and heavy red lines give the energy flux in the 1.5–12 keV (ASM) and 20–300 keV (BATSE) bands, respectively. (b) The corresponding time dependencies of the effective 3–12 keV (blue) and 20–300 keV (red) photon indices. Note occasional gaps in the coverage, joined by straight lines.

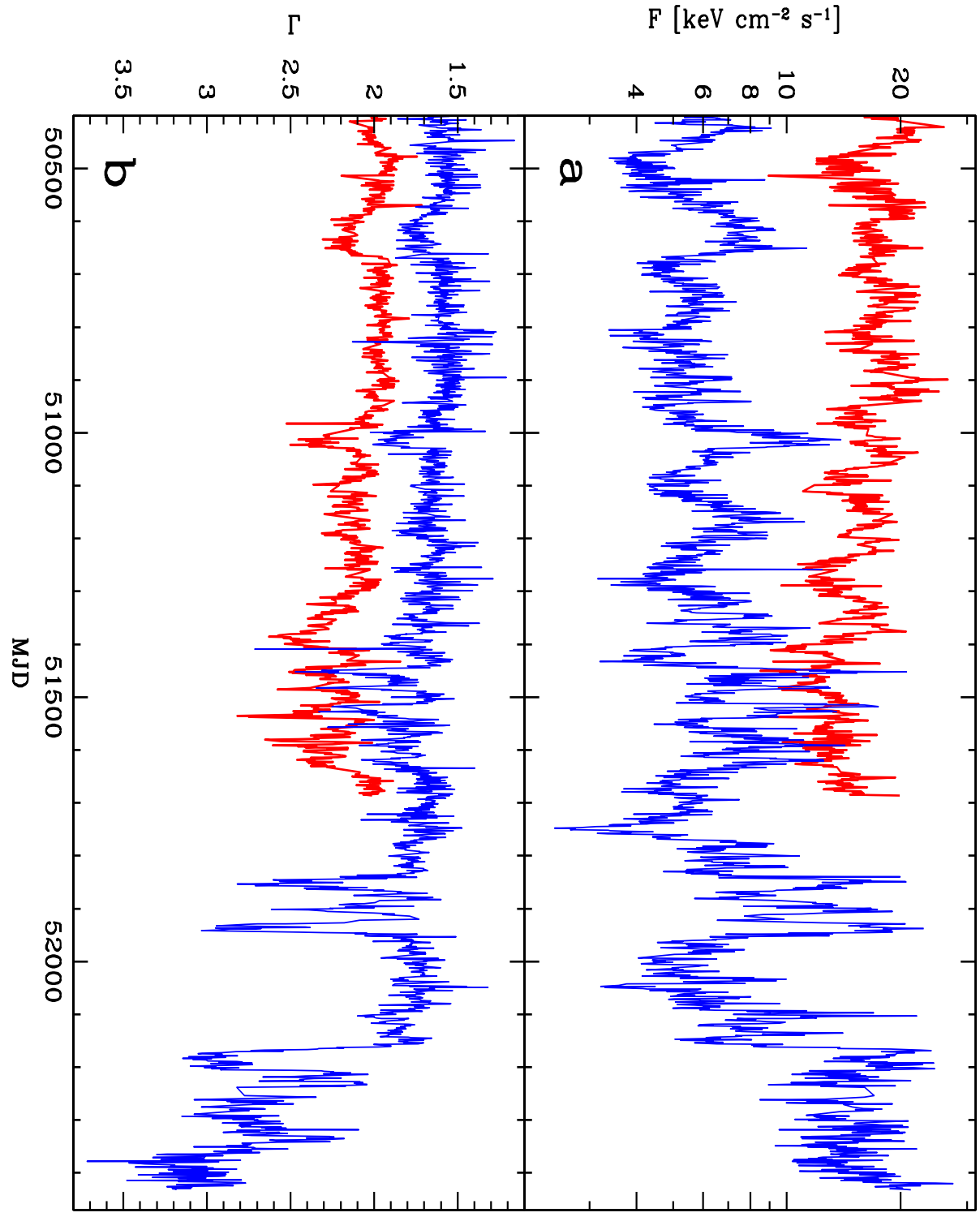


Fig. 1.— continued.

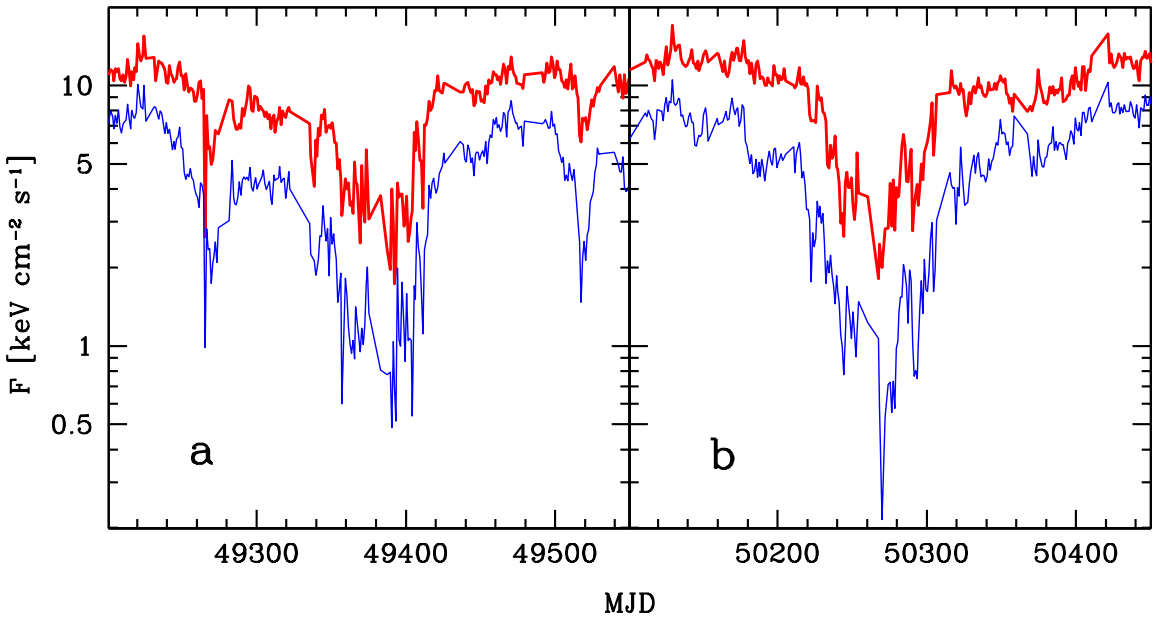


Fig. 2.— Comparison of the state transitions observed by BATSE in (a) 1994 and (b) 1996. The thick (upper) and thin (lower) curves give the 20-100 keV and 100–300 keV energy fluxes. The two transitions show a striking similarity.

to MJD between approximately 50230 and 50307 (1996 May 27–Aug. 12). These definitions may differ somewhat from other ones used in the literature.

Wen et al. (1999) found strong correlations of the ASM flux and hardness with the orbital phase within the hard state, with a peak of the hardness and a dip in the flux around the phase zero (i.e. the companion star in front of the X-ray source), see also Brocksopp et al. (1999a). This effect appears to be due to absorption by a partially ionized wind from the companion. On the other hand, no phase modulation has been found in the soft state. In order to distinguish between this effect and an intrinsic spectral variability, we separately consider the hard state data in the orbital phase between 0.85 and 0.15 and outside this phase interval. We use the ephemeris of Brocksopp et al. (1999b).

We find the logarithms of the fluxes in the three ASM channels strongly correlate with each other, linearly within each state. However, the coefficients for each of the linear dependence are different in each of the three states, as well as the ones for the 1996 soft state are different than those for the 2000–02 soft states. This type of variability is most conveniently shown on flux-index diagrams (analogous to color-magnitude diagrams in stellar astrophysics), Figures 4a, b.

In Figures 4a, b, we see two distinct branches: one formed by the hard state, and the other one corresponding to the soft states, connected by the intermediate state. The hard state is slightly extended towards low fluxes and hard spectra due to local absorption close to the phase zero. Since the bound-free opacity of cosmic medium generally decreases towards increasing energies, the phase effect on the index and flux in the 3–12 keV range is significantly weaker than on those in the 1.5–5 keV one. However, it is clear that absorption can by no means explain the very strong hardness-flux anticorrelation in the hard state. A similar hardness-flux anticorrelation is commonly seen in Seyferts (e.g., Nandra et al. 2000), including some radio-loud ones (e.g., Zdziarski & Grandi 2001).

We note that the negative correlation in the 1.5–5 keV range is stronger than that in the 3–12 keV range, but the latter correlation is still relatively strong. This behavior is consistent with the spectrum pivoting at an energy above the ASM

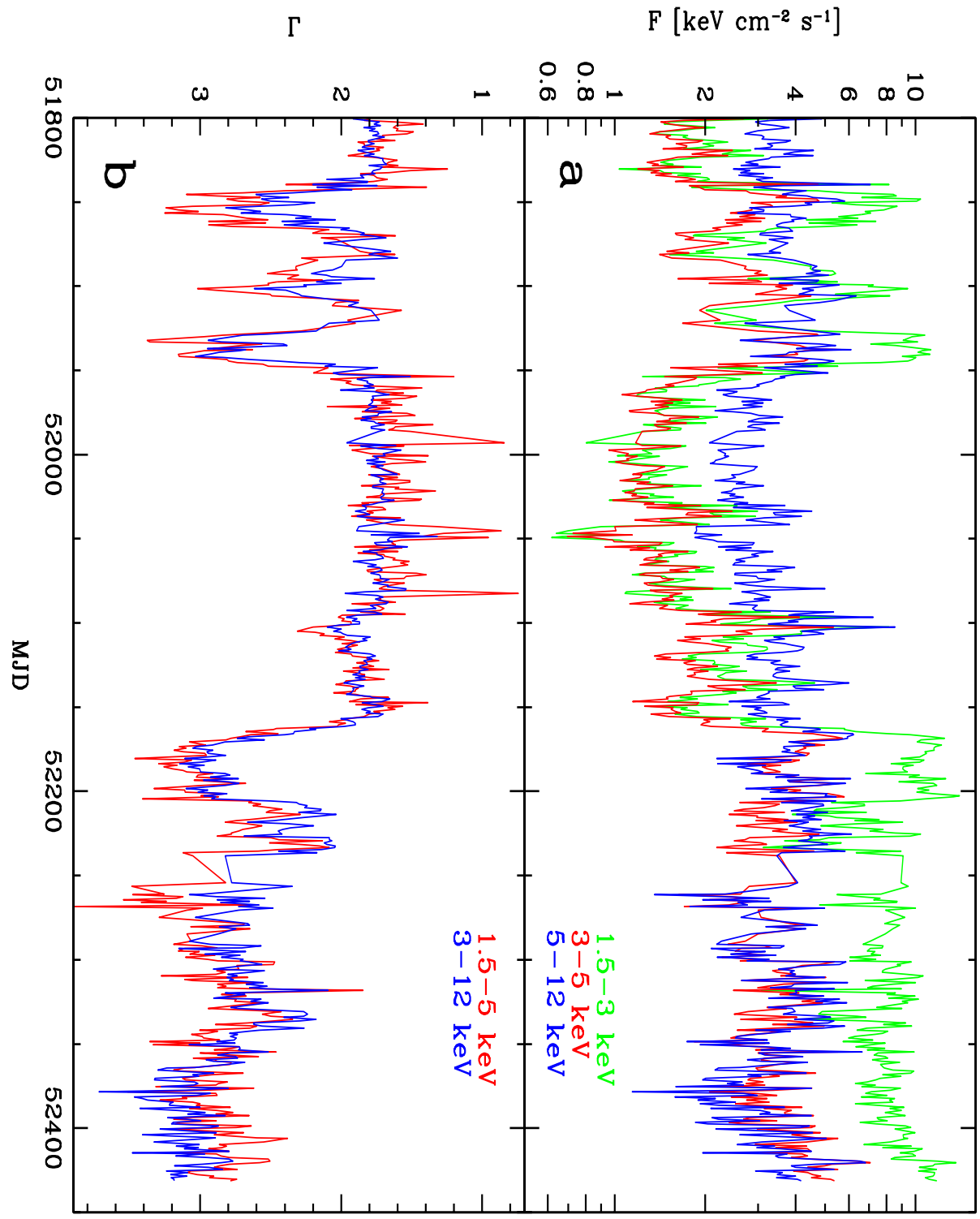


Fig. 3.— (a) Recent ASM light curves of Cygnus X-1, with the 1.5–3 keV, 3–5 keV, and 5–12 keV fluxes shown in green, red, and blue lines, respectively. (b) The corresponding time dependencies of the effective 1.5–3 keV (red) and 3–12 keV (blue) photon indices.

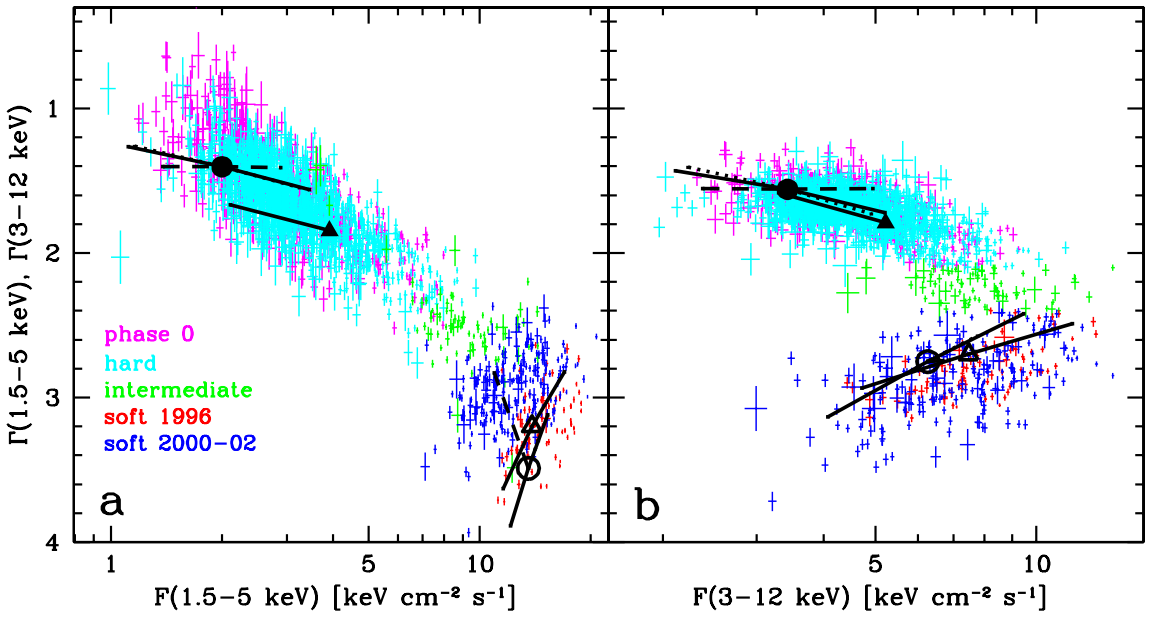


Fig. 4.— The relations between the effective ASM spectral indices [eq. (1)] and the corresponding fluxes in the energy ranges of (a) 1.5–5 keV and (b) 3–12 keV. Two main spectral states are clearly seen (connected by an intermediate state), showing the opposite correlations between the hardness and the flux. The colors red, blue, green, cyan, and magenta correspond to the 1996 soft state, the 2000–02 soft states, the intermediate state [$\Gamma(3-12\,\mathrm{keV}) = 2.1$–$2.4$], and the hard state outside and inside the 0.85–0.15 phase, respectively. The open triangles and circles, and filled triangles and circles correspond to four spectra from pointed observations from 1996 May 30–31, June 22, September 12, 1998 May 3–4, respectively (§6.1). Theoretical variability patterns (§7) are shown hereafter by black solid lines (hard state: constant $L_{\rm hard}$, variable $L_{\rm soft}$; soft state: constant $L_{\rm soft}$, variable $L_{\rm hard}$), dashed lines (hard state: variable total $L$; soft state: variable temperature of seed photons), and the dotted lines (hard state: $e^{\pm}$ pair plasma; soft state: variable $\gamma_{\rm max}$). Some lines on some figures, e.g., the dotted lines in this figure, happen to almost coincide with other lines, and are thus poorly visible.

range. As we find by analyzing the BATSE data, the pivot point is at an energy between 20 and 100 keV. On the other hand, the horizontal spread in Figures 4a, b corresponds to a second variability pattern, in which the X-ray spectrum simply moves up and down without changing its shape. These two variability patterns are explained theoretically in §7.1.

On the other hand, the hardness-flux correlation is positive in the soft states, as found before by Wen et al. (2001). A simple interpretation of this type of variability is a two-component spectrum, with a constant component at low energies (e.g., a blackbody or a disk blackbody) and a variable high-energy tail. Then, the stronger the tail, the higher the flux and the less of the blackbody cutoff is observed, making the spectrum harder. A theoretical interpretation of this behavior is given in §7.2.

We note that the existence of two main branches in the index-flux dependence is independent of the conversion from counts to energy units. If we plot the analogous figures for the raw ASM counts, the obtained shapes are similar to those in Figure 4, see Reig et al. (2002).

Given the above dependencies, there is a strong linear correlation between the spectral indices in the 3–12 keV and 1.5–5 keV energy ranges. Figure 5 shows a comparison of the two quantities, analogous to color-color diagrams often shown for X-ray binaries. However, unlike neutron-star binaries showing changes in the sign of this correlation

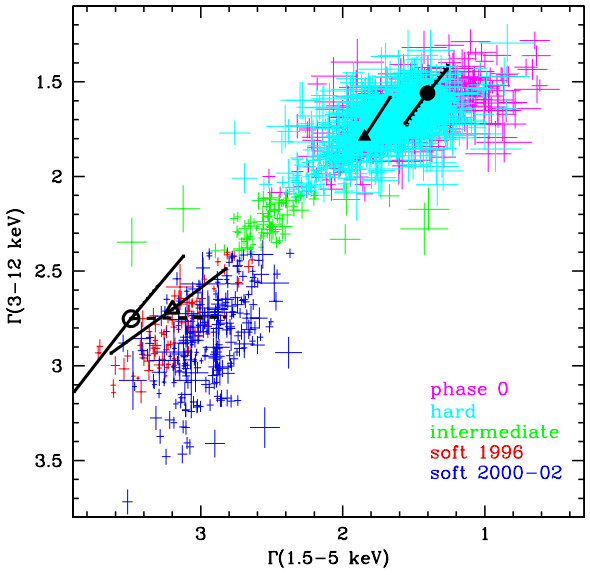


Fig. 5.— The color-color diagram for Cygnus X-1. The black symbols/lines have the same meaning as those in Fig. 4.

(e.g., Schulz, Hasinger, & Trümper 1989), here the two hardnesses (or Γ) are positively correlated in all states, with only the linear coefficients being state-dependent. Thus, the X-ray variability of Cygnus X-1 is only on the diagonal branch of its color-color diagram.

Interestingly, the 2000–02 soft states show distinctly different dependencies between the two indices and the 1.5–5 keV index and flux from those for the 1996 soft state. In Figures 4a and 5, we see that Γ(1.5−5 keV) is generally lower (i.e., the spectrum is harder) and the flux is lower at a given hardness during the 2000–02 soft states. On the other hand, Figure 4b shows that the 3–12 keV fluxes and slopes during the two periods of the soft state are rather similar, but extending to lower fluxes and softer spectra. Also, the flux-hardness correlations in the later soft states remain positive. We discuss theoretical explanation of the differences between the two soft states in §7.3 below.

By inspection of Figure 1, we see that Cygnus X-1 in its hard state can spend hundreds of days (e.g., MJD 50700–50900) with its X-ray flux changing only by a factor of two and Γ(3–12 keV) changing only by ±0.1. If a random time interval of 100 days is chosen within the hard state, the corresponding flux-index points would, in most cases, occupy a relatively small region within the diagonal hard-state strips in Figures 4a, b. The relatively large spread of the indices and fluxes within the hard state seen in these figures is mostly due to the flares and dips in the long-term X-ray light curve. Thus, although the overall anticorrelation between the flux and hardness is extremely strong, it is achieved only on very long time scales, of at least a year. The uniformity of this anticorrelation also indicates that the minor flares/dips in the light curve still belong to the hard state, indicating some common underlying physics (see §7.1). On the other hand, flux changes by a factor of two (corresponding to the horizontal spread of the region covered by the hard-state data in Fig. 4) occur on a time scale of tens of days or less. This explains the lack of a noticeable hardness-flux correlation within time intervals of 5.6 day (i.e., the orbital period) found by Wen et al. (2001).

In the soft states (especially the 1996 one), the correlated flux-index changes occur on a much shorter time scale of a day or so, as clearly seen in Figure 1. Thus, although the overall soft-state flux-hardness correlation is much weaker than the hard-state anticorrelation in Figures 4a, b, the former can be measured on much shorter time intervals, in agreement with the very strong correlation within 5.6-day intervals found by Wen et al. (2001).

### 4.2. The BATSE data

Now, we consider the BATSE data alone. We have found that the spectral state can be best defined for these data using the 100–300 keV flux (see Fig. 2). We then define the hard state by $F(100-300\,\mathrm{keV}) > 3.0$ keV cm$^{-2}$ s$^{-1}$, and the soft state by $F(100-300\,\mathrm{keV}) < 2.2\,\mathrm{keV\,cm^{-2}\,s^{-1}}$, with the intermediate state in between. These definitions are in good agreement with those adopted for the ASM during the period of the simultaneous ASM-BATSE coverage (e.g., the 1996 soft state in the BATSE data corresponds to MJD 50232–50305, very similar to the range obtained from the ASM data in §4.1).

Figure 6a shows the effective 20–300 keV spectral index as a function of the 20-100 keV flux. In the hard state, we still see some anticorrelation between the hardness and flux, qualitatively similar to those in the 1.5–12 keV range. However,

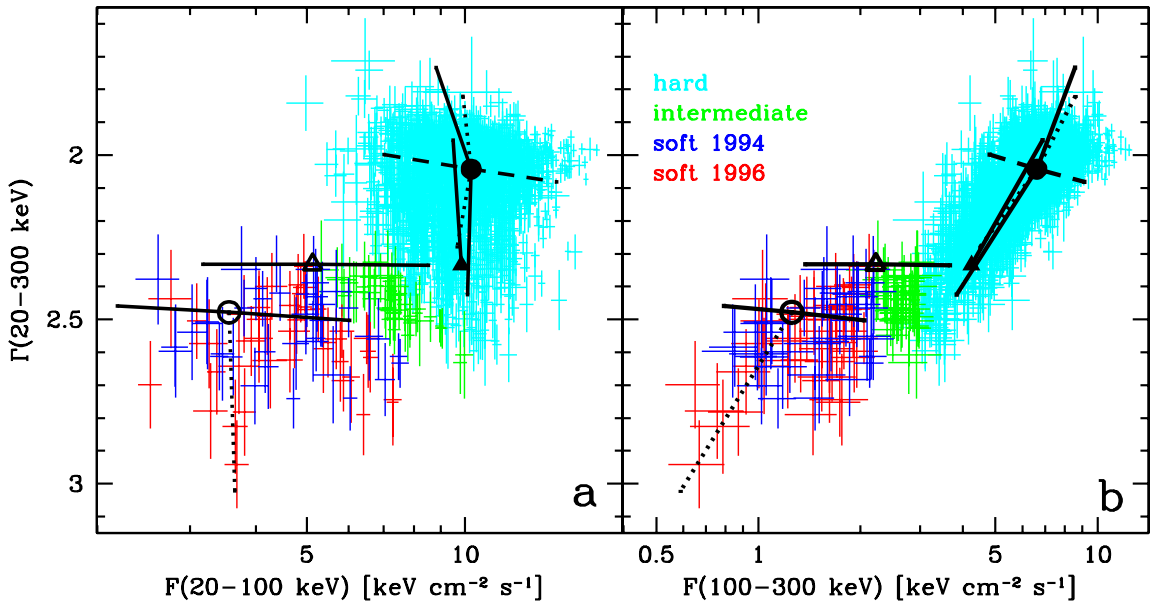


Fig. 6.— The relations between the effective BATSE spectral index [eq. (1)] and the fluxes in the channels (a) 20–100 keV; (b) 100–300 keV. The colors blue, red, green, and cyan correspond to the 1994 soft state, the 1996 one, the intermediate state, and the hard state, respectively. The black symbols and lines have the same meaning as those in Fig. 4, except for the dashed lines in the soft state (specific for the 2000–02 state transitions), which are not shown hereafter.

the anticorrelation is only weak, and, in particular, much weaker than the one for the 3–12 keV range (which, in turn, was weaker than that for the 1.5–5 keV range). We then see in Figure 6b that the 20–300 keV hardness becomes strongly *positively* correlated with the 100–300 keV flux. This behavior shows that the variable spectrum pivots at an energy $\lesssim 100$ keV.

The positive hardness-flux correlation in the 100–300 keV range in the hard state is also seen for the fitted spectral index in that range, as shown in Figure 7. Also, almost no correlation is seen for these quantities in the 20–100 keV range. This shows that the pivoting effect is not an artifact of our use of the effective 20–300 keV index. On the other hand, the fitted indices bear rather large statistical uncertainties. This prevents seeing any trends in the soft states (Fig. 7), where the BATSE fluxes are low and the number of days limited.

Similarly to the case of the ASM data, substantial variations in the range covered by the source on the $\Gamma$-$F$ diagram during the hard state occur on long time scales. If, for example, we consider a typical 100-day interval during the hard state, the corresponding data points would cover a relatively small part of the cyan region in Figures 6a, b.

Figure 8 shows then the relationship between the 20–100 keV and 100–300 keV fluxes. We see that, in spite of the pivoting of the spectrum in the hard state in the BATSE energy range, the two fluxes are still positively correlated. This appears to be due to two effects. First, the pivot point is below 100 keV, and a part of the 20–100 keV flux will still positively be correlated with the 100–300 keV flux. Second, in addition to the pivoting pattern of variability, there is also variability with the spectrum simply moving up and down, as discussed in §4.1.

We also note that BATSE hardness ratio, $F(100-300\,\mathrm{keV})/F(20-100\,\mathrm{keV})$ [related to the effective spectral index used here via eq. (1)] shows significant variations by a factor of 3 in the hard state. This supports earlier findings of Stern et al. (2001).

In the soft state, $\Gamma(20-300\,\mathrm{keV})$ is only weakly changing and roughly independent of

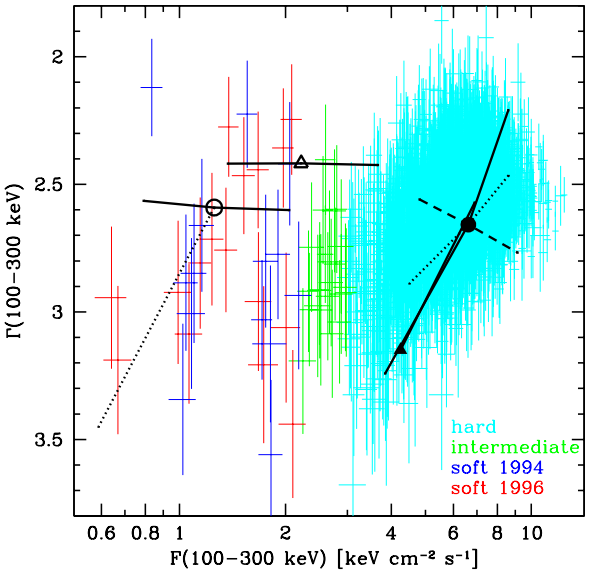


Fig. 7.— The relation between the BATSE spectral index fitted in the 100–300 keV range with the corresponding flux. The black symbols/lines have the same meaning as those in Fig. 4.

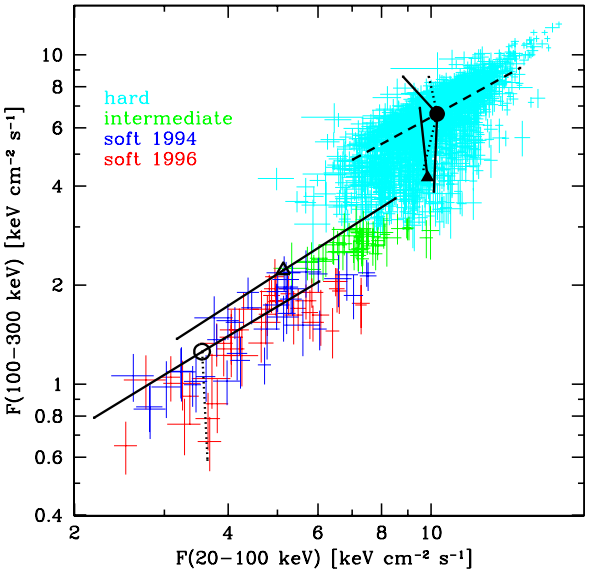


Fig. 8.— The relations between the BATSE fluxes in the 20–100 keV and 100–300 keV energy ranges. The black symbols/lines have the same meaning as those in Fig. 4.

$F(20-100\,\mathrm{keV})$, see Figure 6a. This shows that the 20–100 keV spectrum simply moves up and down with relatively small changes of the spectral shape, consistent with our interpretation of the variability in the ASM range being caused by the amplitude variability of the high-energy tail. In the 20–100 keV range, only the tail (moving up and down) is observed. This behavior is also consistent with the strong positive correlations of the two BATSE fluxes seen in Figure 8.

Finally, there appears to be also a weak positive correlation between $\Gamma(20-300\,\mathrm{keV})$ and $F(100-300\,\mathrm{keV})$ in the 1996 soft state, see Figure 6b. This indicates that the spectrum above 100 keV softens at low flux levels (as indeed seen directly in the lightcurve, see Fig. 2). This points to the existence of a second variability pattern in the 1996 soft state, consisting of a softening of the slope of the tail when the tail amplitude is low.

### 4.3. ASM-BATSE correlations

We consider now the combined ASM-BATSE data. In general, virtually all quantities are strongly correlated with each other, in spite of the different specific times at which the two instruments measure the emission of Cygnus X-1 within a given day. This shows that the intraday variability is relatively weak compared to the variability on longer time scales. We define here the states based on $\Gamma(3-12\,\mathrm{keV})$ (as in §4.1).

In Figure 9b, we compare the fluxes in the lowest and the highest energy channels, i.e., 1.5–3 keV vs. 100–300 keV. We see that they are anticorrelated in the hard state. On the other hand, the 100–300 keV flux is completely independent of the soft X-ray flux in the soft state. In Figure 9a, we see that the 20–100 keV flux becomes weakly positively correlated with the 1.5–3 keV flux in the hard state, while it remains independent of it in the soft state.

These correlations in the hard state are consistent with the spectrum pivoting at an energy of $\lesssim 100$ keV. In the soft state, the lack of correlation of the BATSE fluxes with the 1.5–3 keV one shows that the existence of a constant component at low energies and a variable and independent component at high energies. These findings are consistent with those obtained above while considering the ASM and BATSE data separately.

Figures 10a, b present the ASM-BATSE flux-index diagrams analogous to those for Figures 4

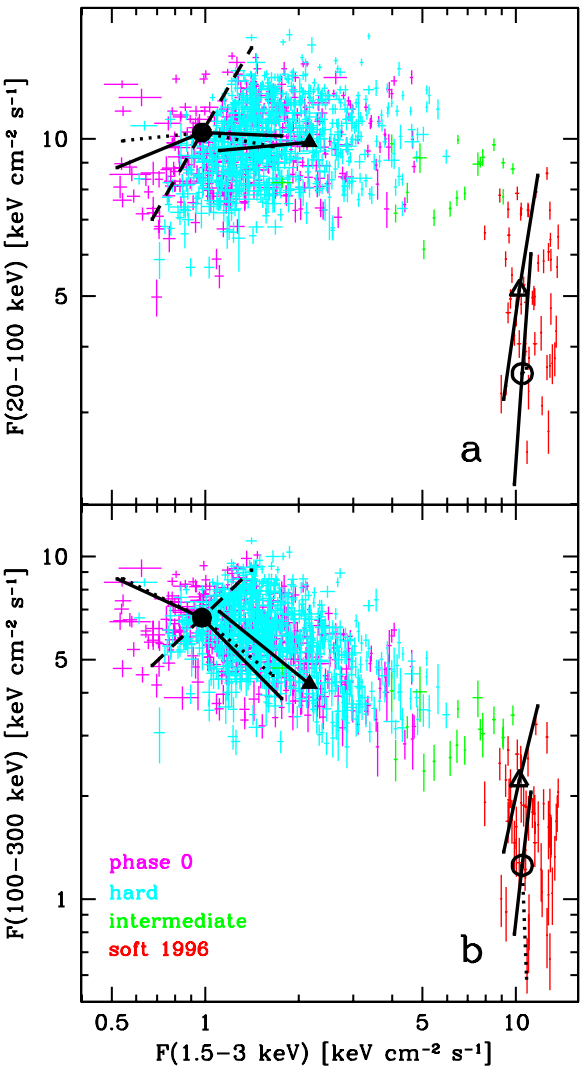


Fig. 9.— The correlation of the ASM 1.5–3 keV flux with the BATSE fluxes: (a) 20–100 keV, (b) 100–300 keV. The meaning of black symbols/lines is the same as that in Fig. 4.

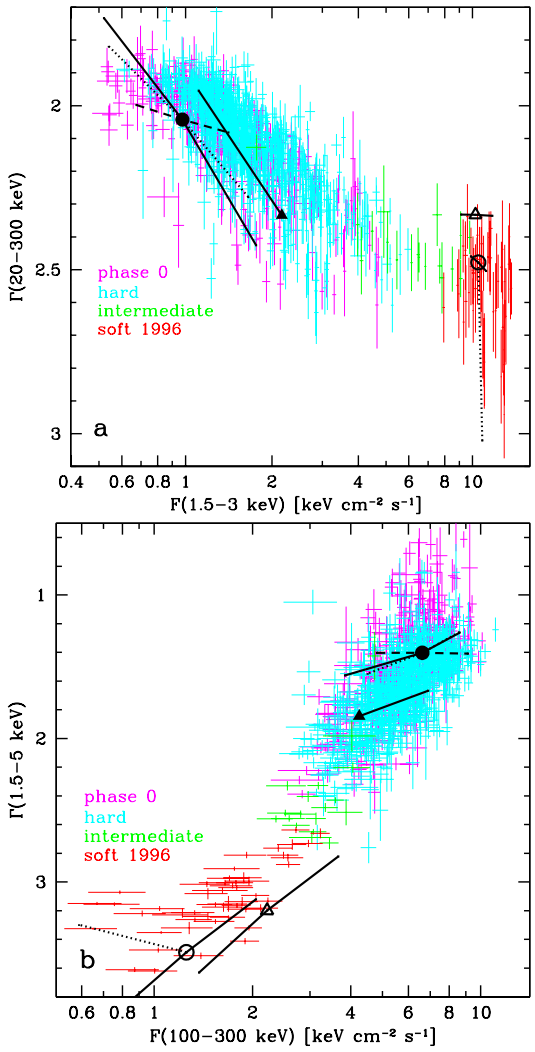


Fig. 10.— ASM-BATSE flux-index correlations. (a) $\Gamma(20-300\,\mathrm{keV})$ vs. $F(1.5-3\,\mathrm{keV})$; (b) $\Gamma(1.5-5\,\mathrm{keV})$ vs. $F(100-300\,\mathrm{keV})$. The meaning of black symbols/lines is the same as that in Fig. 4.

for the ASM data alone. Figure 10a shows that, in the hard state, the dependence of the BATSE hardness on the ASM flux is similarly anticorrelated as that of the ASM index on the ASM flux (Fig. 4). In the soft state, $\Gamma(20-300\,\mathrm{keV})$ is uncorrelated with the ASM flux, as well as it shows a substantial spread of values.

On the other hand, the 1.5–5 hardness is now *positively* correlated in the hard state with $F(100-300\,\mathrm{keV})$ (Fig. 10b), opposite to the case of the ASM data alone. This is again consistent with existence of a pivot point below 100 keV, reversing the correlation with respect to that with a flux at energies $\ll 100$ keV. On the other hand, there is a moderate hardening of the ASM spectrum with the increasing $F(100-300\,\mathrm{keV})$ in the soft state. This is explained by changing of the amplitude of the high energy tail with a constant soft, blackbody component which dominates the ASM flux.

Figure 11 shows an ASM-BATSE index-index correlation. The 3–12 keV hardness is positively

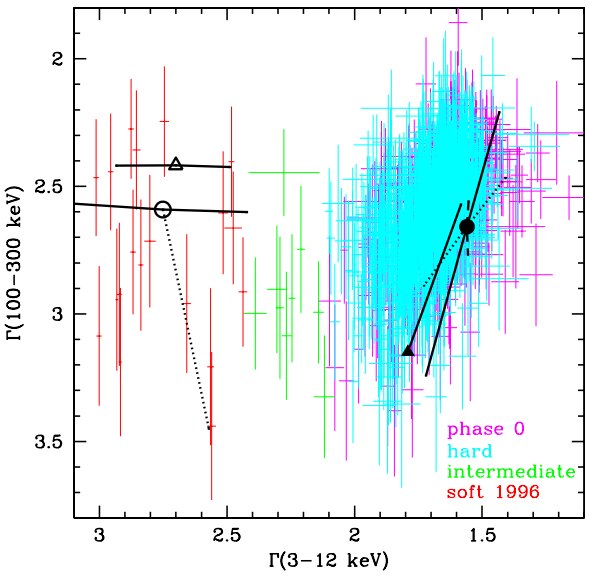


Fig. 11.— The correlation between the 3–12 keV and 100–300 keV indices. The black symbols/lines have the same meaning as those in Fig. 4.

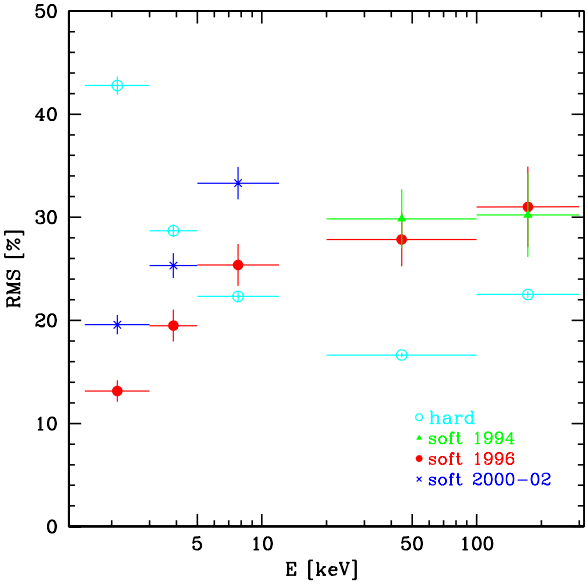


Fig. 12.— The relative rms variability as a function of energy in the hard state and in the 1994, 1996 and 2000–02 soft states. The respective error bars are identified by the open circles, filled triangles, filled circles and diagonal crosses, respectively.

correlated with the 100–300 keV one in the hard state, showing that the spectrum changes its local slope in the same direction at all measured energies. The BATSE index is substantially softer than that of the ASM, showing that the spectrum at a given time softens with increasing energy. On the other hand, there is no correlation in the soft state. This means that the tail component varies independently of the blackbody one.

## 5. Fractional Variability

An independent way of quantifying the variability of Cygnus X-1 is to consider the fractional variability as a function of energy. The intrinsic (i.e., after relatively small corrections for the measurement errors) root mean-square (rms) variability based on one-day averages in the entire data sets is 89%, 48%, 26%, 21%, 30% in the 1.5–3, 3–5, 5–12, 20–100, and 100–300 keV energy ranges, respectively (see relatively similar values obtained by Z97 for a period including the 1996 state transtion). However, this variability includes the state transitions. As we have found in §4 above, the spectral variability indicates different physical mechanisms operating in the two main states. Thus, we have computed the rms variability separately in the hard state (defined as above and excluding the phase range of 0.85–0.15 for the ASM data) and in the 1994, 1996 and 2000–02 soft states. The results are shown in Figure 12.

The rms dependence in the hard state is consistent with our finding of a pivot point in the 20–100 keV range, where the relative variability has the minimum. The maximum variability is in the softest channel, consistent with the variability being driven by a variable input of soft seed photons (see §7). On the other hand, the dependence in the 1996 soft state is consistent with a constant soft component and a variable tail with almost constant shape. Also, the 1994 soft state (not observed by the ASM) has very similar values of the rms, confirming our previous finding of the two states being very similar to each other. On the other hand, the 2000–02 soft states show an offset of the rms values with respect to those of the 1996 soft state. We have checked that it is not due to varying properties of the relatively large number of soft episodes during 2000–02. In particular, the rms values for only the most recent soft

state (MJD $> 52250$) are even larger than those shown on Figure 12. A possible explanation for the offset is a decrease of the characteristic energy of the constant soft component (see §7.3), which then moves the rms pattern to lower energies. In addition, the rms of the high-energy tail in the recent soft states appears higher than that in the 1996 soft state.

In the hard state, the shown values of rms correspond to the frequency range of $\sim 10^{-8}$–$10^{-5}$ Hz. It is highly interesting to compare the power in the variability on those long time scales with that corresponding to short time scales. The rms values corresponding to seven *RXTE*/PCA observations in the hard state are given by Lin et al. (2000). They obtain the rms for 0.002–10 Hz in the 2–50 keV energy range of $\sim$ 20–40% (with a relatively flat energy dependence, consistent with the variability at a constant spectral shape), i.e., values very similar to those obtained by us. On the other other hand, the high-frequency hard-state power spectrum per log of frequency of Cygnus X-1 has an overall maximum (usually with two nearby peaks) in the $\sim$ 0.1–10 Hz range and it declines fast both towards lower and higher frequencies (e.g., Gilfanov, Churazov, & Revnivtsev 1999). This implies that the broad-band hard-state spectrum of Cygnus X-1 has at least two maxima with comparable power, one at $\sim$ 1 Hz, and one somewhere below $10^{-5}$ Hz.

## 6. Pointed Observations

Further insight into the character of spectral variability of Cygnus X-1 can be gained from comparing spectra from pointed observations taken at different times. Here we discuss information that can be derived from spectral variability between those observations and luminosities in different states.

### 6.1. Spectra

Figure 13 shows three broad-band spectra in the hard state, two in the soft state, and one in the intermediate state. The triangles and circles in Figures 4–11 correspond to four of those pointed spectra (1996 May 30–31, June 22, September 12, 1998 May 3–4).

In the hard state, we see two patterns of spectral variability. First, the 1991 June (black) and 1998 May (blue) spectra are almost parallel to each other, and vary only in the normalization being different by a factor of $\sim 1.5$. (Note that this 1991 spectrum is thus at about highest daily flux observed by BATSE.) Such a pattern was also seen within the 1991 observation, when the four spectra taken within one day (with each observation lasting $\sim$ 2 hours) varied only in the normalization within a factor of $\lesssim 2$ (G97). We can identify this type of variability with the spread in the $F$-$\Gamma$ correlations in §4 at constant values of $\Gamma$, e.g., clearly seen in both the ASM (Fig. 4) and BATSE (Fig. 6) data.

Second, the 1996 September hard-state spectrum (cyan) is substantially softer than the other hard-state spectra and its high-energy cutoff is at a visibly lower energy. In a thermal Comptonization fit (see §7 below), $kT \simeq 57$ keV whereas $kT \simeq 86$ keV and 77 keV in the 1991 June 6 and 1998 May 3–4 spectra, respectively. The cyan and blue spectra intersect at $\sim$ 50 keV. We can identify this type variability with the hardness-flux anticorrelation seen in the ASM data (Fig. 4), and the anticorrelation between the soft and hard X-ray fluxes (Fig. 9b).

In the soft and intermediate states, we see the tail (in the red, magenta and green spectra) moves up and down with relatively small changes in the spectral shape. The soft X-ray peak is almost the same in the two soft-state spectra (red and magenta), but the form of the intermediate spectrum above 3 keV implies a decrease of that peak in the intermediate state. Also, when the tail moves up, the X-ray spectrum hardens. These effects are consistent with the behavior of the soft and intermediate state ASM spectra (Fig. 4).

### 6.2. Bolometric fluxes and the nature of the state transitions

One of the outstanding puzzles of Cygnus X-1 has been the small difference, claimed to be $\lesssim$ 50–70% (Z97) between the bolometric fluxes in the hard and the soft states. This requires fine-tuning of the hard-state accretion rate as well as fine-tuning of models of the transition (Esin et al. 1998). However, we stress here that the estimate by Z97 was based on their estimates of the effects of absorption and the bolometric fluxes based solely on the ASM and BATSE data.

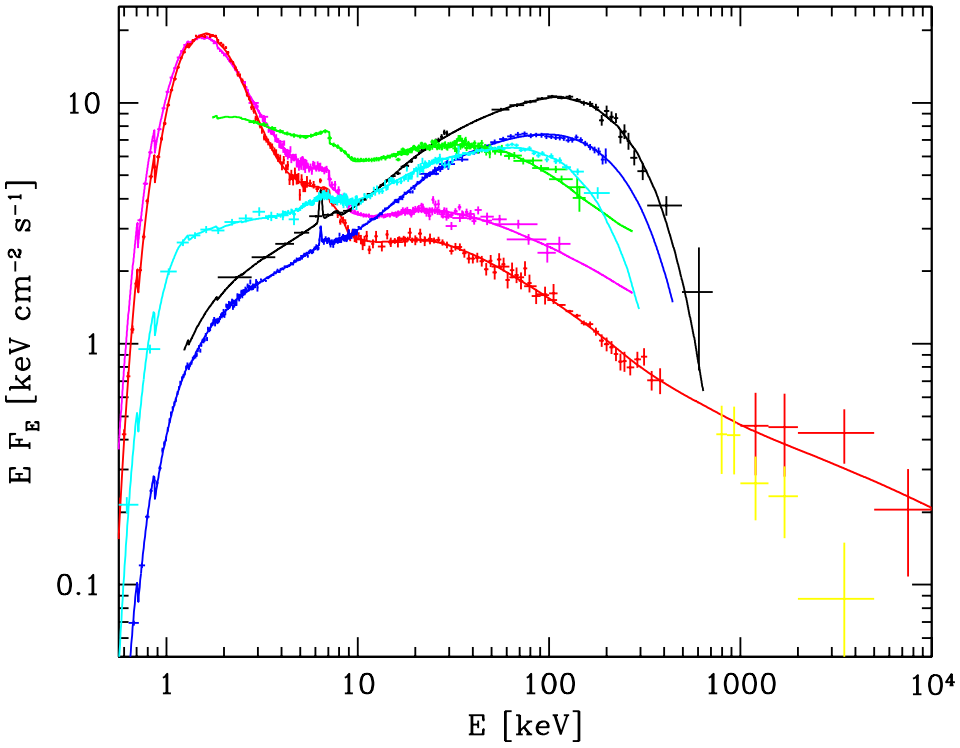


Fig. 13.— Example broad-band spectra from pointed observations. The hard state: symbols in black: the *Ginga*-OSSE spectrum from 1991 June 6, no. 2 in G97; blue: the *BeppoSAX* spectrum from 1998 May 3–4 (D01); cyan: the *BeppoSAX* spectrum from 1996 September 12 (F01). The soft and intermediate states: red: the *BeppoSAX* spectrum from 1996 June 22 (F01) shown together with a *CGRO*/OSSE and COMPTEL spectra from 1996 June 14–25 (M02); magenta: the *ASCA*-*RXTE* spectrum of 1996 May 30–31 (G99); green: the *RXTE* spectrum of 1996 May 23 (G99). Table 1 gives the detectors to which the spectra are normalized. The solid curves give the best-fit Comptonization models (thermal in the hard state, and hybrid, thermal-nonthermal, in the other states, see §7). For the *RXTE* spectra, we have updated the PCA response to that of 2002 February. The symbols in yellow show the average hard-state 0.75–5 MeV spectrum observed by *CGRO*/COMPTEL (M02).

To make further progress, we have compiled in Table 1 the intrinsic bolometric fluxes of Cygnus X-1 based on a number of highly accurate broad-band pointed observations, including those described in §6.1. Those data provide much better estimates of the unabsorbed bolometric flux than those possible with the ASM-BATSE data. We see that whereas the typical flux in the hard state is $\sim$ 4–5 $\times$ $10^{-8}\,\mathrm{erg\,cm^{-2}\,s^{-1}}$, it is $\gtrsim$ 1.5 $\times$ $10^{-7}\,\mathrm{erg\,cm^{-2}\,s^{-1}}$ in the soft state, i.e., $\sim$ 3–4 times *higher*. We also note that the two spectra with the highest hard-state fluxes correspond to either the peak of intraday variability or a relatively soft continuum. Also, the flux in the intermediate state is just between those in the two main states. The fact that the total *observed* flux during the 1996 state transition remains almost unchanged (see Fig. 1), as pointed out by Z97, can be reconciled with the results in Table 1 by noting that whereas the effect of absorption on the measured bolometric flux is negligible in the hard state (with the spectrum peaking at $\sim$ 100 keV, Fig. 13), it becomes crucial in the soft state, and very difficult to estimate with the ASM data alone (with the peak of the $EF_E$ spectrum at $\sim$ 1 keV).

This result makes models of the state transitions based on a change of the accretion rate, $\dot{M}$, much more viable than with the previous result

TABLE 1

BOLOMETRIC FLUXES AND CORRESPONDING ISOTROPIC LUMINOSITIES

| Date | State | $F^{a}$ | $L^{b}$ | Satellite(s) | Detector[c] |
|---|---|---|---|---|---|
| 1991–1994[d] | hard | 3.80 | 1.82 | *CGRO* | OSSE |
| 1991 June 6 | hard | 3.26–5.92[e] | 1.56–2.83 | *Ginga*-*CGRO* | OSSE |
| 1996 May 23 | intermediate | 9.80 | 4.69 | *RXTE* | PCA |
| 1996 May 30–31 | soft | 15.4 | 7.38 | *ASCA*-*RXTE* | PCA |
| 1996 June 22 | soft | 15.1 | 7.24 | *BeppoSAX*-*CGRO* | LECS |
| 1996 Sept. 12 | hard | 6.27 | 3.00 | *BeppoSAX* | LECS |
| 1998 May 3–4 | hard | 4.42 | 2.12 | *BeppoSAX* | MECS |
| 1998 Oct. 4–5 | hard | 4.40[f] | 2.11 | *BeppoSAX* | MECS |

[a]The unabsorbed bolometric flux of the model in units of $10^{-8}\,\mathrm{erg\,cm^{-2}\,s^{-1}}$.

[b]The corresponding luminosity assuming isotropy and a distance of 2 kpc (see G99) in units of $10^{37}\,\mathrm{erg\,s^{-1}}$.

[c]The detector to which the flux is normalized.

[d]Using the average *CGRO* spectrum of the hard state of M02 and a broad-band model with a correction (+7% derived using *BeppoSAX* data) for the presence of a soft excess.

[e]The flux range during that day in four observations (G97); the spectrum shown in Fig. 13 corresponds to the highest flux.

[f]C. Done, private communication.

of Z97. In particular, a relatively large fraction of the accretion flow in the hard state advected (e.g., Narayan & Yi 1995) or forming outflows (e.g., Blandford & Begelman 1999), i.e., not efficiently radiating, becomes now possible.

## 7. Theoretical Interpretation

We interpret here the spectral variability of Cygnus X-1 in terms of Comptonization of soft X-ray blackbody seed photons. We use a Comptonization code by Coppi (1992, 1999), with its present XSPEC (Arnaud 1996) version (`eqpair`) described in G99. This model was also used to fit both states of Cygnus X-1 by Poutanen & Coppi (1998), and some states of GRS 1915+105 by Zdziarski et al. (2001). In general, the electron distribution can be purely thermal or hybrid, i.e., Maxwellian at low energies and non-thermal at high energies in the presence of an acceleration process. The electron distribution, including the temperature, $kT$, is calculated self-consistently from the luminosities in Comptonized photons, $L_{\rm hard}$, and in the blackbody seed photons irradiating the cloud, $L_{\rm soft}$. The plasma optical depth, $\tau$, includes a contribution from $e^{\pm}$ pairs (which may be negligible or not). The importance of pair production depends on the ratio of the luminosity to the characteristic size, $r$, which is usually expressed in dimensionless form as the compactness parameter, $\ell \equiv L\sigma_{\rm T}/(rm_{\rm e}c^3)$ (where $\sigma_{\rm T}$ is the Thomson cross section and $m_{\rm e}$ is the electron mass). We also include Compton reflection (Magdziarz & Zdziarski 1995) and Fe K fluorescent lines. We refer the reader to G99 for details.

We fit this model to the spectra from pointed observations (§6.1). Using the obtained models, we calculate the energy fluxes in the bands corresponding to those of the ASM and BATSE. The fluxes from the pointed observations have uncertainties negligible compared to those of the monitoring instruments and are very weakly dependent on the assumed model, given the energy resolution of the pointed instruments being much less than the width of any of the ASM-BATSE energy bands. Then, in order to compare theoretical variability patterns with those observed, we change some parameters in some of the best-fit models, and recalculate the fluxes. For the fitted BATSE indices, we create simulated BATSE data with models of pointed observations and theoretical models, and fit them with a power law

spectrum. We use two BATSE responses corresponding to the extreme orientations of the detector with respect to the source and average the resulting indices. However, the differences in the two values of $\Gamma$ are $\lesssim 0.03$, i.e., negligibly small.

### 7.1. The hard state

In the hard state, the Comptonizing plasma is nearly thermal (G97; Poutanen 1998; Zdziarski 2000). The electron distribution may contain a weak high-energy tail, but its contribution to spectral formation below several hundred keV is negligible (M02). If the compactness is low enough for pair production being negligible, the main parameters of a model are $\tau$, $L_{\rm hard}$, and $L_{\rm soft}$.

We have found that we can explain the anticorrelation of the X-ray flux and hardness (§4.1) by a variable luminosity of seed blackbody photons, $L_{\rm soft}$, irradiating a cloud of thermal plasma with an approximately constant energy dissipation rate (given by $L_{\rm hard}$) and a constant $\tau$. Under these conditions, the plasma electron temperature, $kT$, will adjust itself to the variable seed flux as to satisfy energy balance. Then, the higher the seed flux, the lower $kT$, and (since a decrease of $kT$ at a constant $\tau$ corresponds to an increase of $\Gamma$) the softer the X-ray spectrum. Since the Comptonized spectrum joins at low energies to the peak of the spectrum of the seed photons, this will also correspond to an increase of the soft X-ray flux. The pivoting of the spectrum will occur somewhere below 100 keV causing the decrease of the high energy flux above 100 keV.

We have applied this model to the two hard-state observations of Cygnus X-1 by *BeppoSAX* (1996 Sept. 12, F01; 1998 May 3–4, D01), see §6.1. As discussed in those papers, Cygnus X-1 shows a soft X-ray excess in addition to the main thermal Comptonization component. The soft excess is well modeled by an additional Comptonization region. The seed photons are blackbody at a temperature of $\sim$ 0.15 keV. This model provides a good fit to either of the data sets, as shown in Figure 13. The position of these data in Figures 4–11 are shown by the filled triangles and circles, respectively. We note that there may be some offsets of the *BeppoSAX* points with respect to the corresponding ones from ASM and BATSE due to calibration uncertainties (see Appendix A) and intraday variability.

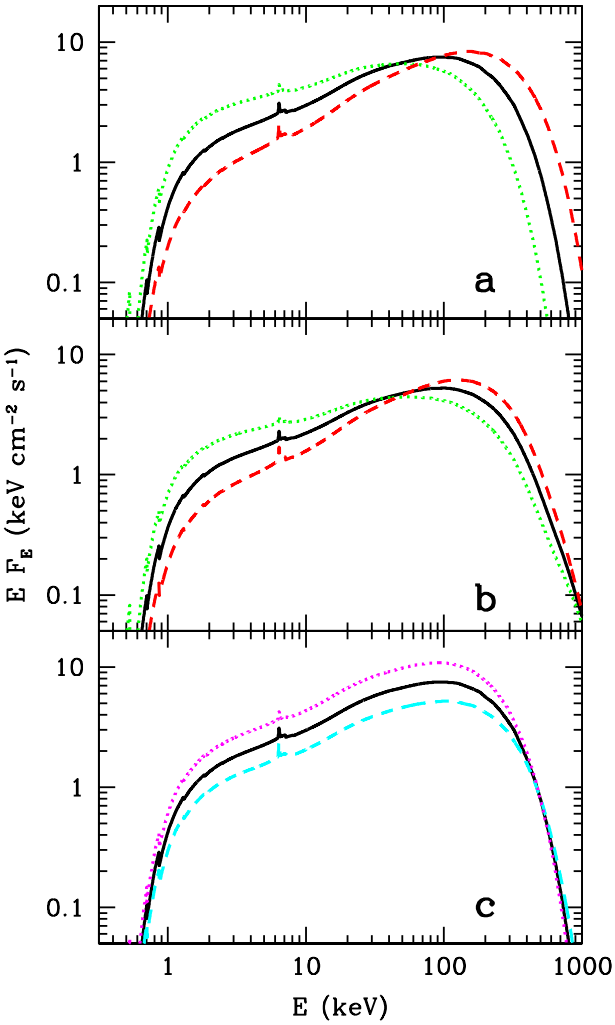


Fig. 14.— The variability patterns (dashed and dotted curves) predicted by our models in the hard state induced by varying seed soft photon flux in (a) an $e^-p$ plasma; (b) $e^\pm$ pair-dominated plasma, and (c) by a change in the bolometric luminosity due to the change of the local accretion rate. The middle solid curves correspond to the respective best fits to the 1998 May *BeppoSAX* observation.

We then vary only $L_{\rm soft}$ for each of the Comptonization regions, increasing and decreasing it by a factor of 2, and keep the compactness at a low enough value for pair production to be negligible. We do not adjust the model normalization. The predicted spectra for the 1998 May observation are shown in Figure 14a. We see the pivot point

at $\sim$ 50–90 keV. The resulting predictions for the fluxes and the spectral hardness are shown in Figures 4–11 by the solid black lines originating at the filled symbols (corresponding to the actual observations). In the case of the 1996 September observation, we show only the effect of the decreasing $L_{\rm soft}$ (i.e., hardening of the X-ray spectrum) since the observed spectrum is already rather soft, see Figure 13. Given the simplicity of our assumption, the agreement with the observed spectral variability is rather good, yielding support to the picture of the X-ray variability driven by a variable flux of irradiating soft X-ray photons. A possible accretion geometry corresponding to this variability pattern is shown in Figure 15 (see, e.g. Poutanen, Krolik, & Ryde 1997; Esin et al. 1998, Zdziarski 1998), and its discussion in given in §7.4.

The above model is the same as the one used to explain the X-ray spectral variability of 3C 120 by Zdziarski & Grandi (2001). Note that the pivot obtained for 3C 120 is at $\sim$ 7–10 keV, which difference is due to both the power-law component of 3C 120, $\Gamma \simeq 1.9$, softer than $\Gamma \sim 1.7$ typical for the hard state of Cygnus X-1, and the lower energy of the seed photons in AGNs than in black-hole binaries. Specifically, UV seed blackbody photons with a temperature of 10 eV were assumed for 3C 120, compared to $\sim$ 150 eV fitted for the hard state of Cygnus X-1.

We note that an increase/decrease of $\Gamma$ in this model corresponds to a substantial decrease/increase of $kT$, in the $\sim$ 60–100 keV range in the case shown in Figure 14a. Such an effect is seen when we compare the two hard-state *BeppoSAX* spectra. The softer and the harder one have $kT \simeq 57$ keV and 77 keV, respectively. However, we do not know how universal this correlation is, and the BATSE data are of insufficient accuracy to test this effect.

On the other hand, the hot Comptonizing plasma may be $e^\pm$ pair dominated. If it is mostly thermal, no signature of annihilation will be visible in the spectra (Zdziarski 1986; Maciołek-Niedźwiecki, Zdziarski, & Coppi 1995). Thus, we cannot detect the presence of pairs just by the spectral shape. However, their presence will have an effect on the spectral variability. Namely, a variable $L_{\rm soft}$ will cause changes in the pair production rate causing changes in the total Thomson optical depth, $\tau$. Pairs act as a thermostat (e.g., Malzac, Beloborodov, & Poutanen 2001). We have fitted a pair-dominated model (achieved at a high enough compactness, $\ell \simeq 500$ and assuming a nonthermal fraction of 5% consistent with the results of M02) to the 1998 May data, and then changed $L_{\rm soft}$ by a factor of 2 as in the case of $e^-p$ plasma. Indeed, the equilibrium $kT$ stayed almost constant at 72 keV in all three cases. The resulting variability pattern is shown in Figure 14b. We see that the obtained spectra indeed show no annihilation features (while pair annihilation is included in the `eqpair` model). The predictions of this model are shown by the dotted lines connected to the filled circle in Figures 4–11. We see that the present data are not sensitive enough to determine which of the two cases is preferred.

As we discussed in §4, there has to be another variability pattern in the hard state when the total luminosity varies with a more or less constant spectral shape. If the X-rays in Cygnus X-1 are produced in a hot inner accretion flow (as in Fig. 15), a higher accretion rate (and higher luminosity) corresponds to a higher optical depth, $\tau$, of the hot disk. If the geometry of the flow does not change, i.e., the feedback from the cold disk is constant, the seed photon luminosity (from the outer cool disk) is linearly proportional to the total luminosity. The resulting spectrum is then almost independent of luminosity, except that the high energy cutoff decreases with an increase of $\tau$ since the electron temperature will be adjusted to keep the Comptonization parameter $y \equiv 4\tau kT/m_{\rm e}c^2$ constant (see e.g. Poutanen 1998 for a review).

We simulate this variability pattern by increasing and decreasing the total luminosity by $\sqrt{2}$ starting from the same *BeppoSAX* spectra of Cygnus X-1 and, at the same time, adjusting $\tau$ (with no pairs) according to predictions of models of hot accretion disks. If $y =$ constant, $\tau \propto L^{2/7}$ and $L^{1/6}$ in the advection and cooling dominated cases (Zdziarski 1998). Here we assumed the former. A decrease of $kT$ with increasing $L$ at a constant $\Gamma$ (since $y$ is constant) is consistent with the four data sets of G97, as well as it has been observed in two bright states of the black hole binary GX 339–4 (Zdziarski 2000; Wardziński et al. 2002). As we noted above this variability pattern should have a smaller amplitude comparing with the first pattern. The resulting spectra are shown in Figure 14c. The observed spectra that show

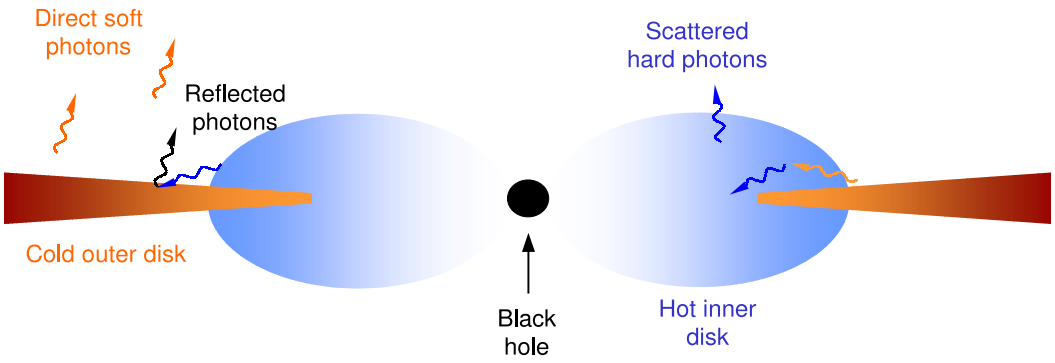


Fig. 15.— A schematic representation of the likely geometry in the hard state consisting of a hot inner accretion flow surrounded by optically-thick accretion disk. The disk is truncated far away from the minimum stable orbit, but it overlaps with the hot flow. The soft photons emitted by the disk are Compton upscattered in the hot flow, and emission from the hot flow is partly Compton-reflected from the disk. The main long-term variability of Cygnus X-1 appears to be due to the variable truncation radius, causing changes in the hardness of the X-ray spectrum. In a second pattern, the local accretion rate through the flow changes while the geometry remains constant.

similar variability are the hard state spectra (the black and blue ones) in Figure 13. The resulting predictions for the fluxes and the spectral slopes are shown in Figures 4–11 by the dashed lines connected to the filled circle. We can see that the two patterns describe well the full range of observed correlations.

We note that these two variability patterns give opposite predictions for the dependence of $kT$ on the flux at $\sim 200$ keV. In the case of varying $L_{\rm soft}$, $kT$ either increases or remains constant when flux increases, and the opposite is true for the case of varying the total $L$.

### 7.2. The 1996 soft state

For the 1996 soft state, we use the *ASCA-RXTE* observation (G99) and the *BeppoSAX-CGRO* one (F01; M02). In those papers, the data were already fitted with the `eqpair` model, in which a hybrid, thermal-nonthermal plasma Comptonizes seed, blackbody photons coming from an accretion disk (with the maximum blackbody temperature of $kT_{\rm soft}$. Now a substantial part ($\sim 0.7$ in those two observations) of the dissipation in the Comptonizing cloud goes into particle acceleration, in addition to thermal heating (see G99 for details). The points corresponding to those observations are shown by the open triangles and circles, respectively, in Figures 4–11.

Then, we vary $L_{\rm hard}$ by a factor of 1.5 up and down while keeping $L_{\rm soft}$ constant. The predicted spectra are shown in Figures 16a, b. This qualitatively explains the spectral variability in the soft-state region in Figures 4–11 as shown by the solid lines extending from the open symbols (corresponding to the actual observations). This variability pattern corresponds to a stable optically-thick accretion disk (Shakura & Sunyaev 1973) and variable flares on its surface. A likely corresponding accretion geometry is shown in Figure 17, and more discussion in given in §7.4. The disk in Cygnus X-1 is thermally and viscously stable (G99), supporting this picture. The model of constant disk and a variable tail component has also been found by Churazov, Gilfanov, & Revnivtsev (2001) to fit *RXTE*/PCA data for Cygnus X-1.

However, the above variability pattern of variable $L_{\rm hard}$ cannot explain the correlation of the BATSE spectral slope with the 100–300 keV flux (Figs. 2 and 6b) as well as substantial variability of that slope (Fig. 10a). We note that a softening of the $\sim$ 50–500 keV spectrum with decreasing flux in the same energy range has also been observed by OSSE between two observations in the soft states in 1994 and 1996 (G99).

We have tested a number of models to explain this secondary variability pattern, with variable either the power-law index of the accelerated elec-

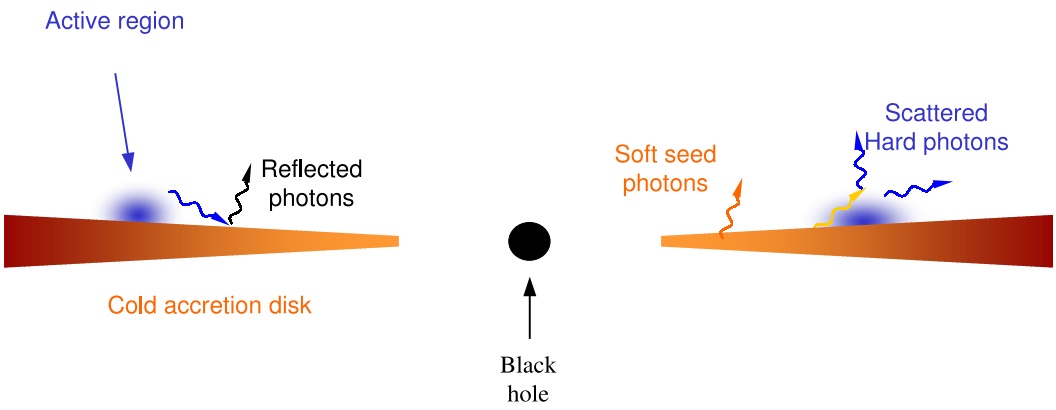


Fig. 17.— A schematic representation of the likely geometry in the soft state consisting of flares/active regions above an optically-thick accretion disk extending close to the minimum stable orbit. The soft photons emitted by the disk are Compton upscattered in the flares, and emission from the flares is partly Compton-reflected from the disk. In the case of Cygnus X-1, the disk is stable whereas the power supplied to the flares is variable during the duration of the soft state.

trons, the fraction of the energy which goes to the acceleration, and the variable maximum Lorentz factor, $\gamma_{\rm max}$, of the accelerated electrons. We have found the first pattern does not provide a good fit to the data at all, whereas the last one provides the best fit. Changes of $\gamma_{\rm max}$ have little effect on the slope or the flux at low energies (in the ASM range), but markedly affect the BATSE fluxes and the slope. Starting from the best-fit model for the 1996 June data, we decrease $\gamma_{\rm max}$ from $10^3$ to 10. The resulting spectrum is shown by the dotted curve in Figure 16c. The corresponding predictions for the correlation diagrams are shown for the 1996 June spectrum only by the dotted lines in Figures 4–11.

### 7.3. The 2000–02 soft states

As shown in §4.1 and 5, the 2000–02 soft states show different spectral and timing properties from those of the 1996 soft state. In particular, Figure 12 shows an offset between the two ASM rms dependencies. In the framework of the above soft-state model (§7.2) consisting of two components, a constant disk soft blackbody and a variable tail, the rms offset is stronly suggestive of a reduction of the disk color temperature. Then, the variable tail starts to dominate at correspondingly lower energies. From Figure 12, we estimate the reduction of the characteristic color temperature, $kT_{\rm soft}$, to be by a factor of $\sim$ 1.5–2.

This inference is, in fact, supported by the ASM colors. As shown in Figures 4 and 5, the later soft states have harder 1.5–5 keV spectra, as well as of a lower flux at a given hardness. This is consistent with a decrease of $kT_{\rm soft}$, in which case the 1.5–5 keV range has now a larger contribution from the tail, which has a harder spectrum than the high-energy cutoff of the disk blackbody, dominant in 1996 up to $\sim$ 3 keV (see Fig. 16b).

We have modeled this behaviour using the `eqpair` model. Starting from the best-fit model for the 1996 June data, we decreased $kT_{\rm soft}$ from 370 eV (the best fit value) to 200 eV. This, indeed, has led to a hardening of the 1.5–5 keV spectrum. However, we also found that the 3–12 keV hardens as well, contrary to the data. This implies some change of the parameters of the Comptonizing plasma in addition to a reduction of $kT_{\rm soft}$. Unfortunately, the ASM data alone hardly constrain the shape of the Comptonization spectrum. Here, we found we can account for the ASM data by a purely phenomenological assumption of setting the reflection fraction to zero. We stress, however, that the actual character of the change of the hot plasma can only be determined by broad-band (from soft to hard X-rays) pointed observations (which were not available to us). E.g, the power-law index of the accelerated electrons, the fraction of the energy which goes to the acceleration, or $\gamma_{\rm max}$ could have changed.

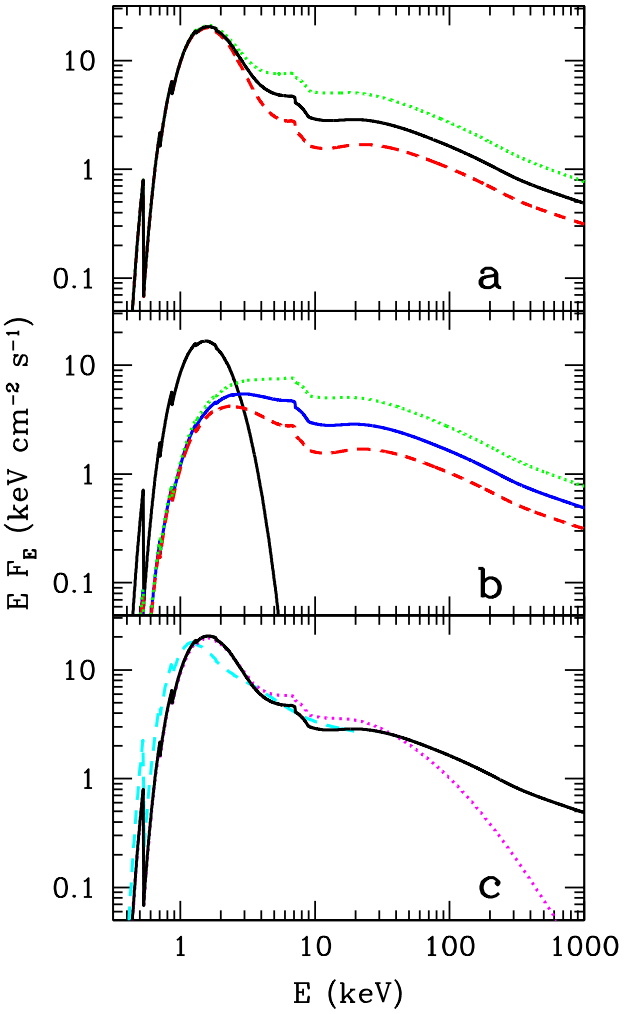


Fig. 16.— (a) The primary variability pattern for the soft state. The dotted and dashed curves show the variability induced by varying hard luminosity while keeping the seed luminosity constant. (b) The constant blackbody and variable tail components shown separately. (c) The dotted curve illustrates the secondary variability pattern, due to the maximum Lorentz factor of the accelerated electrons being reduced from $\gamma_{\rm max} = 10^3$ (assumed for the solid curve) to 10. The dashed curve shows the effect of decreasing the disk temperature, which can explain the difference in the 2000–02 soft states with respect to that of 1996. The solid curve in all panels correspond to the best fit to the 1996 June *BeppoSAX-CGRO* spectrum.

The resulting effect on the 1.5–5 and 3–12 keV slopes is shown by the dashed line originating at the open circle in Figures 4–5. We see that indeed we can qualitatively account for the changes of the color and fluxes from the 1996 soft state to the 2000–02 ones. The corresponding spectrum is shown by the dashed curve in Figure 16c. We show this spectrum only for energies $\lesssim$ 20 keV, since we cannot make any predictions for higher energies based on the ASM data alone.

Note that we adjusted the normalization of the spectrum to match the data. We also note the decrease of the disk temperature is not accompanied by a correspondingly large decrease in the luminosity, as seen, e.g., in Figures 1 and 3. This is possible if the temperature decrease was not caused by an increasing accretion rate but by a change of some physical conditions of the disk causing the color correction (the ratio of the color temperature to the effective one) to decrease. Any more detailed explanation of the changes requires pointed observations in the soft X-ray range.

The spectral variability *within* the 2000–02 soft states appears to follow the primary pattern found for the 1996 soft state, i.e., changes of $L_{\rm hard}$ at a constant $L_{\rm soft}$. We do not show this pattern separately in Figures 4–5 for the sake of clarity.

### 7.4. Discussion

Table 2 summarizes our findings above. We stress that the primary variability patterns in the hard and soft states are modelled by *opposite* behaviors of the hard and soft luminosities. This argues agains spectral models of the state transition related to a quantitative change of one parameter while keeping the geometry constant, e.g., variations in the relative fraction of the power dissipated in a disk corona (e.g., Young et al. 2001). Although the overall spectrum in the hard and soft states is indeed hard and soft, respectively, their spectral variability patterns are completely different.

In the soft state, the spectral variability is indeed fully consistent with the presence of flares (forming a corona) on the surface of an accretion disk, as schematically shown in Figure 17. The luminosity in the flares is strongly variable while that in the underlying disk is approximately constant. On the other hand, it is likely that the

TABLE 2
SUMMARY OF SPECTRAL VARIABILITY OF CYGNUS X-1

| State | Variability pattern | Model | Likely physical cause |
|---|---|---|---|
| Hard | Variable $\Gamma$ with a pivot at $\sim 50$ keV | Variable $L_{\rm soft}$, constant $L_{\rm hard}$ | Hot inner flow irradiated by a variable outer disk |
| Hard | Variable amplitude at $\sim$ constant shape | Variable total $L$ | Variable local $\dot{M}$ |
| Soft | Variable tail on top of a constant soft component | Constant $L_{\rm soft}$, variable $L_{\rm hard}$ | Nonthermal flares above the inner disk |
| Soft | Softening at $\gtrsim 50$ keV at low fluxes | Less acceleration at low $L_{\rm hard}$ | Unknown physics of the flares |

power in the flares is derived from dissipation in the underlying disk. In that case, $L_{\rm hard} + L_{\rm soft}$ would be approximately constant rather than just $L_{\rm soft}$. We have modelled this variability pattern as well, and have found it completely consistent with the data but barely distinguishable from the one for constant $L_{\rm soft}$ shown in Figures 4–11. Thus, we do not show it for the sake of simplicity. The 1996 and 2000–02 soft states both follow the variability pattern driven by changes of $L_{\rm hard}$, but the latter show the disk blackbody temperature lower than that of the former (see §7.3).

In contrast, the primary variability in the hard state corresponds to a variable flux in the seed photons while keeping the power supplied to electrons in the hot plasma approximately constant. In our opinion, the most likely geometry appears to be a hot inner flow surrounded by an overlapping thin, optically-thick, accretion disk supplying the soft photons, as schematically shown in Figure 15. Changes in the inner radius of the disk cause then variable flux of seed photons. The seed photons are likely to be mostly due to reprocessing of the hard radiation. As noted in §4, this variability takes place on rather long time scales, which are apparently needed to change the outer disk. On the other hand, changes in the local $\dot{M}$ in the hot disk cause the overall spectrum to move up and down, but with a constant shape determined by the approximately constant geometry.

An increase in the global $\dot{M}$ then causes a decrease in the inner radius of the outer disk, which is compatible with some physical scenarios (e.g., Esin et al. 1998). The data do allow a modest increase of $L_{\rm hard}$ (instead of its constancy) with increasing $\dot{M}$, but the present data are not sensitive enough to test it. When the thin disk moves close to the minimum stable orbit, the hot accretion flow collapses and is replaced by the active regions above the thin disk.

On the other hand, it is also possible that the hot plasma forms active coronal regions above a disk also in the hard state. The variable $L_{\rm soft}$ can be then related to changes in the bulk velocity of the active regions/flares (Beloborodov 1999; Malzac et al. 2001) and a constant power dissipated in the flares causes then the constancy of $L_{\rm hard}$. However, the reversal of this variability pattern in the soft state needs then to be explained.

We note that, for the sake of simplicity, we have neglected the well-known correlation between the spectral index and Compton reflection (Zdziarski, Lubiński, & Smith 1999; Gilfanov et al. 1999, 2000). These changes of the reflected component would have a relatively minor effect on our results. We stress, however, that the above correlation is completely consistent with the flux-hardness anticorrelation in the hard state. Namely, the cold medium providing the soft seed photons is most likely the same one as the reflecting medium (see Fig. 15). Then an increase of the flux of soft photons due to reprocessing of the hard radiation would also be accompanied by an increase of the reflection strength. Thus, the presence of one of those correlations makes it likely that the other

one is also present.

## 8. Conclusions

We have presented the history of the flux and hardness of Cygnus X-1 from the entire course of its monitoring by the BATSE, and up to 2002 June by the ASM. In particular, we show in detail the ASM data from the recent soft states (MJD 51840 till 52431).

We find then numerous correlations between various ASM-BATSE fluxes and indices. In the hard state, we find the X-ray flux at $< 12$ keV and $> 100$ keV to be negatively and positively, respectively, correlated with the hardness in the same energy range. We find this is compatible with the variable slope of the overall spectrum and a pivot at $\sim 50$ keV. This behavior is well modeled by thermal Comptonization in a hot plasma with an approximately constant power irradiated by a variable flux of soft seed photons.

In all of the soft states, the X-ray flux at $< 12$ keV is positively correlated with the hardness (as earlier found by Wen et al. 2001). However, in the case of the 1996 soft state, the correlation disappears above 20 keV, where the spectrum undergoes flux changes at an approximately constant shape. This is well modeled by hybrid, thermal/nonthermal Comptonizationin a hot plasma with a variable power irradiated by soft seed photons with a constant flux, i.e., the behavior opposite to that in the hard state. In addition, we find the overall 1.5–300 keV spectrum is moving up and down in the hard state, and the high energy tail in the soft state softens at low flux levels. The four patterns are summarized in Table 2.

We also compute the fractional variability amplitude as a function of photon energy in the two states. In the hard state, it has a minimum at the 20–100 keV range, consistent with the presence of the spectral pivot at $\sim 50$ keV, and the maximum at the 1.5–3 keV range, consistent with the variability being driven by a variable soft flux. In the soft state, the fractional variability is lowest in the 1.5–3 keV range and increases strongly towards higher energies, consistent with the presence of a stable soft (disk) component and a variable high-energy tail.

Our preferred model of the accretion flows in the hard state is an inner hot flow overlapping with an outer thin accretion disk with a variable inner radius. That variability is responsible for varying flux of seed photons and changes of the spectral slope. However, a dynamic corona above a cold disk is also possible. In both scenarios, variations of the local accretion rate at the constant geometry are then responsible for the changes of the luminosity occuring at an approximately constant shape. In the soft state, the data are fully compatible with variable nonthermal flares occuring above a stable thin disk.

We also study in detail differences between the 1996 and 2000–02 soft states. We find the ASM spectra of the latter to be harder in the 1.5–5 keV range and to have the rms variability significantly higher. Both effects can be modeled by a decrease of the color disk temperature from the 1996 soft state to the 2000–02 ones. On the other hand, we find the 1994 soft state (monitored by BATSE only) to have the same spectral and timing properties at energies $> 20$ keV as the 1996 soft state.

Furthermore, we present a compilation of detailed broad-band spectra of Cygnus X-1 from pointed observations in the hard, soft, and intermediate states. The spectral variability observed in this data set fully supports our conclusions based on the ASM-BATSE data. Furthermore, we find the bolometric luminosity in the spectra from the pointed observations increases by a factor of $\sim 3$–4 from the hard state to the soft state. This amplitude of the changes of $L$ strongly supports models of the state transitions based on a change of the global $\dot{M}$.

This research has been supported by grants from KBN (5P03D00821, 2P03C00619p1,2) and the Foundation for Polish Science (AAZ). JP and AAZ acknowledge support from the Royal Swedish Academy of Sciences and the Polish Academy of Sciences through exchange programs. We thank the ASM and BATSE teams for their efforts in carrying out the monitoring, C. Done and T. Di Salvo for providing us with their *BeppoSAX* data, M. Gierliński for making the original versions of Figures 15 and 17, and G. Wardziński and P. Lachowicz for help with some aspects of the data analysis.

## A. Comparison with Pointed Observations

The ASM results are given in counts per second, $R_i$, in the three adjacent channels, $i = a$, $b$, $c$, which nominal boundaries are 1.5, 3, 5, 12 keV. In general, conversion of those rates into energy flux units is uncertain, and depending on the spectral shape and the position of the source on the sky. Here, we have adopted a simple conversion based on comparison of fluxes from six pointed observations with the ASM average daily fluxes taken on the same days. The pointed observations are listed in Table 1, and correspond to MJD 50226 (*RXTE*, G99), 50233–50234 (*ASCA-RXTE*, G99), 50256, 50338 (*BeppoSAX*, F01), 50936–50937 (*BeppoSAX*, D01), MJD 51091 (*BeppoSAX*, C. Done, private communication). The first five of them are also shown in Figure 13.

We have then assumed a linear dependence of the energy flux from each channel on the count rate in the same one and in a neighbouring one. This takes into account the dependence of the conversion on the hardness of the incident spectra. We have then least-square fitted the conversion coefficients. In each of the three fits, we have given the same relative weight to each of the measurements, in order to avoid the fit being dominated by the data points with the highest flux (i.e., in the soft state). In the case of the channel $b$, we have found that allowing the dependence of the conversion on both neighbouring channel did not improve the fit quality with respect to the dependence on the count rate in the $a$, $b$ channels only.

In this way, we have obtained,

$$\begin{pmatrix} F_a \\ F_b \\ F_c \end{pmatrix} = \begin{pmatrix} 0.2552 & -0.0324 & 0 \\ -0.0357 & 0.2507 & 0 \\ 0 & -0.0533 & 0.3591 \end{pmatrix} \begin{pmatrix} R_a \\ R_b \\ R_c \end{pmatrix} \tag{A1}$$

where $F_i$ and $R_i$ are in units of keV cm$^{-2}$ s$^{-1}$ and cm$^{-2}$ s$^{-1}$, respectively. We see in Figures 18a, b that the resulting overall agreement is very good, given that some of the differences have to be systematic, caused by the pointed observations being not taken exactly on the same times as the ASM observations and by calibration differences between different instruments.

The BATSE fluxes in energy units have been obtained in the way described in §2. Figure 19 shows the comparison with the pointed observations listed above. We see a generally good agreement between the two data sets.

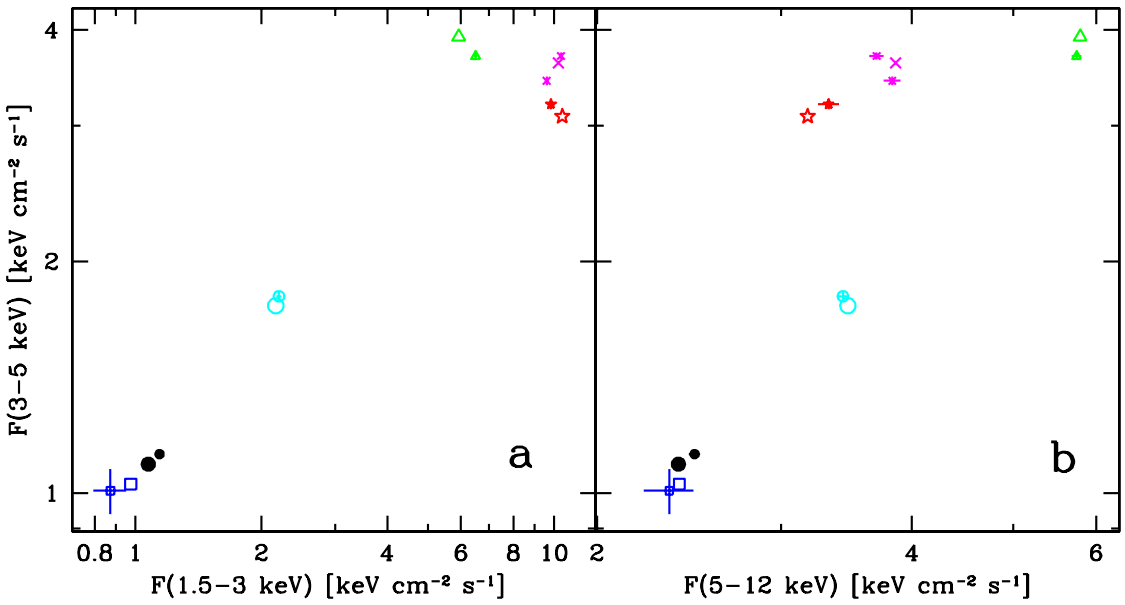


Fig. 18.— Comparison of the fluxes in the three ASM channels (error bars and small symbols) with those of the corresponding pointed observations (large symbols). The data corresponding to the six pointed observations correspond to open triangles, crosses, asterisks, open circles, open squares, and filled circles, in the temporal order.

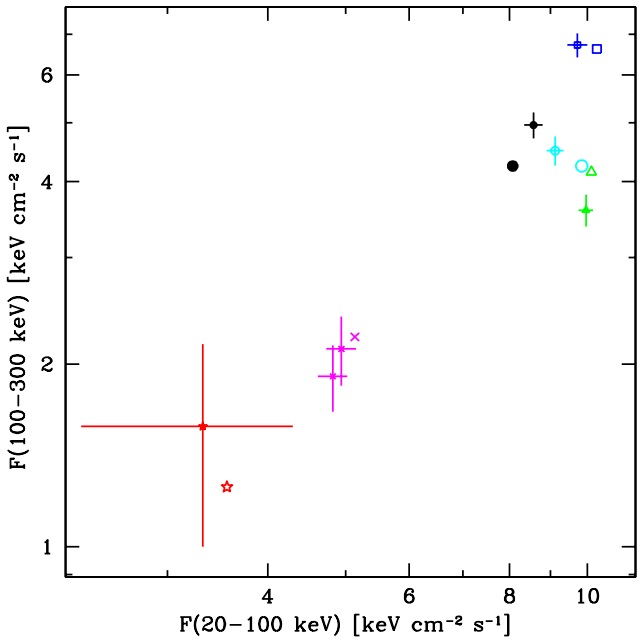


Fig. 19.— Comparison of the fluxes in the two BATSE channels (error bars and small symbols) with those of the corresponding pointed observations (large symbols). The data corresponding to the six pointed observations correspond to open triangles, crosses, asterisks, open circles, open squares, and filled circles, in the temporal order.

## REFERENCES


Abramowicz, M. A., Chen, X., Kato, S., Lasota, J.-P., & Regev, O. 1995, ApJ, 438, L37

Arnaud, K. A. 1996, in ASP Conf. Series 101, Astronomical Data Analysis Software and Systems V, ed. G. H. Jacoby & J. Barnes (San Francisco: ASP), 17

Beloborodov, A. M. 1999, ApJ, 510, L123

Blandford, R. D., & Begelman, M. C. 1999, MNRAS, 303, L1

Bowyer, S., Byram, E. T., Chubb, T. A., & Friedman, M. 1965, Sci, 147, 394

Brocksopp, C., Fender, R. P., Larionov, V., Lyuty, V. M., Tarasov, A. E., Pooley, G. G., Paciesas, W. S., & Roche, P. 1999a, MNRAS, 309, 1063

Brocksopp, C., Tarasov, A. E., Lyuty, V. M., & Roche, P. 1999b, A&A, 343, 861

Churazov, E., Gilfanov, M., & Revnivtsev, M. 2001, MNRAS, 321, 759

Coppi P. S., 1992, MNRAS, 258, 657

Coppi, P. S. 1999, in ASP Conf. Ser. Vol. 161, High Energy Processes in Accreting Black Holes, ed. J. Poutanen & R. Svensson (San Francisco: ASP), 375

Crary, D. J., et al. 1996, ApJ, 462, L71

Cui, W., Feng, Y.-X., & Ertmer, M. 2002, ApJ, 564, L77

Di Salvo, T., Done, C., Życki, P. T., Burderi, L., & Robba, N. R. 2001, ApJ, 547, 1024 (D01)

Esin, A. A., Narayan, R., Cui, W., Grove, J. E., & Zhang, S. N. 1998, ApJ, 505, 854

Frontera, F., et al. 2001, ApJ, 546, 1027 (F01)

Gierliński, M., Zdziarski, A. A., Done, C., Johnson, W. N., Ebisawa, K., Ueda, Y., Haardt, F., & Phlips, B. F. 1997, MNRAS, 288, 958 (G97)

Gierliński, M., Zdziarski, A. A., Poutanen, J., Coppi, P. S., Ebisawa, K., & Johnson, W. N. 1999, MNRAS, 309, 496 (G99)

Gilfanov, M., Churazov, E., & Revnivtsev, M. 1999, A&A, 352, 182

Gilfanov, M., Churazov, E., & Revnivtsev, M. 2000, in Proc. 5th CAS/MPG Workshop on High Energy Astrophysics, ed. G. Zhao et al. (Beijing: China Sci. Techn. Press), 114 (astro-ph/0002415)

Golenetskii, S., Aptekar, R., Mazets, E., Frederiks, D., Cline, T., & Hurley, K. 2002, IAUC 7840

Harmon, B. A., et al. 2002, ApJS, 138, 149

Lin, D., Smith, I. A., Böttcher, M. & Liang, E. P. 2000, ApJ, 531, 963

Maciołek-Niedźwiecki, A., Zdziarski, A. A., & Coppi, P. S. 1995, MNRAS, 276, 273

Magdziarz, P., & Zdziarski, A. A. 1995, MNRAS, 273, 837

Maccarone, T. J., Coppi, P. S., & Poutanen, J. 2000, ApJ, 537, L107

Malzac, J., Beloborodov, A. M., & Poutanen, J. 2001, MNRAS, 326, 417

McConnell, M. L., et al. 2002, ApJ, 572, in press (astro-ph/0112326) (M02)

Nandra, K., Le, T., George, I. M., Edelson, R. A., Mushotzky, R. F., Peterson, B. M., & Turner, T. J. 2000, ApJ, 544, 734

Narayan, R., & Yi, I. 1995, ApJ, 452, 710

Paciesas, W. S., Robinson, C. R., McCollough, M. L., Zhang, S. N., Harmon, B. A., & Wilson, C. A., 1997, in The 4th Compton Symposium, ed. Ch. D. Dermer, M. S. Strickman & J. D. Kurfess (New York: AIP), 834

Poutanen, J. 1998, in Theory of Black Hole Accretion Discs, ed. M. A. Abramowicz, G. Björnsson & J. Pringle (Cambridge: Cambridge Univ. Press), 100 (astro-ph/9805025)

Poutanen, J., & Coppi, P. S. 1998, Physica Scripta, T77, 57

Poutanen, J., Krolik, J. H., & Ryde, F. 1997, MNRAS, 292, L21

Reig, P., Papadakis, I., & Kylafis, N. D. 2002, A&A, 383, 202

Revnivtsev, M., Gilfanov, M., & Churazov, E. 2000, A&A, 363, 1013

Schulz, N. S., Hasinger, G., & Trümper, J. 1989, A&A, 225, 48

Shakura, N. I., & Sunyaev, R. A. 1973, A&A, 24, 337

Smith, D. M., Heindl, W. A., & Swank, J. H. 2002, ApJ, 569, 362

Stern, B. E., Beloborodov, A. M., & Poutanen, J. 2001, ApJ, 555, 829

Wardziński, G., Zdziarski, A. A., Gierliński, M., Grove, J. E., Jahoda, K., & Johnson, W. N. 2002, MNRAS, submitted

Wen, L., Cui, W., Levine, A. M., & Bradt, H. V. 1999, ApJ, 525, 968

Wen, L., Cui, W., & Bradt, H. V. 2001, ApJ, 546, L105

Young, A. J., Fabian, A. C., Ross, R. R., & Tanaka, Y. 2001, MNRAS, 325, 1045

Zdziarski, A. A. 1986, ApJ, 303, 94

Zdziarski, A. A. 1998, MNRAS, 296, L51

Zdziarski, A. A. 2000, in IAU Symp. 195, Highly Energetic Physical Processes and Mechanisms for Emission from Astrophysical Plasmas, ed. P. C. H. Martens, S. Tsuruta & M. A. Weber (San Francisco: ASP), 153 (astro-ph/0001078)

Zdziarski, A. A., & Grandi, P. 2001, ApJ, 551, 186

Zdziarski, A. A., Lubiński, P., & Smith, D. A. 1999, MNRAS, 303, L11

Zdziarski, A. A., Grove, J. E., Poutanen, J., Rao, A. R., & Vadawale, S. V. 2001, ApJ, 554, L45

Zhang, S. N., Cui, W., Harmon, B. A., Paciesas, W. S., Remillard, R. E., & van Paradijs, J. 1997, ApJ, 477, L95 (Z97)


This 2-column preprint was prepared with the AAS LaTeX macros v5.0.